NASA TECHNICAL NOTE

NASA TN D-4757

C.1



NASA TN D-4757



# A SATELLITE VIEW OF TYPHOON MARIE 1966 DEVELOPMENT

*by*

*G. Warnecke and L. J. Allison*
*Goddard Space Flight Center*

*E. R. Kreins*
*USAF Environmental Technical Applications Center*

*and*

*L. M. McMillin*
*Allied Research Associates, Inc.*

NATIONAL AERONAUTICS AND SPACE ADMINISTRATION • WASHINGTON, D. C. • NOVEMBER 1968

# A SATELLITE VIEW OF TYPHOON MARIE 1966 DEVELOPMENT

By G. Warnecke and L. J. Allison

Goddard Space Flight Center
Greenbelt, Md.

E. R. Kreins, Major, USAF

USAF Environmental Technical
Applications Center
Washington, D.C.

L. M. McMillin

Allied Research Associates, Inc.
Concord, Mass.

NATIONAL AERONAUTICS AND SPACE ADMINISTRATION

For sale by the Clearinghouse for Federal Scientific and Technical Information
Springfield, Virginia 22151 – CFSTI price $3.00

## ABSTRACT

A complete documentation of Nimbus II High Resolution Infrared Radiometer data and ESSA-3 photographs is presented for the life-time of Typhoon Marie 1966. Particular emphasis in this analysis was given to the earliest stages of noticeable storm development. The interpretation of the satellite data in combination with the sparse conventional observations from the central Pacific Ocean revealed meteorological conditions in the development area which are commonly found necessary for tropical storm development. These conditions were as follows: the sea surface temperature was above 26.5°C, a deep lower tropospheric moist layer existed, the low level flow was convergent, and the vertical wind shear was small. The distance of the development area from the intertropical convergence was 7 to 8 degrees latitude. The mid-Pacific troughs were present in both hemispheres and outlined by distinct cloud bands that reached with their extremeties into the development area. Additionally, however, it was found that a heavy large-scale cloud system shaped like a boomerang existed slightly to the west. This cloud system consisted of two formerly extratropical frontal cloud bands that penetrated into the subtropical and tropical regions from both hemispheres and met close to the equator. Both features were associated with a pronounced upper tropospheric (200-mb) divergence that was mainly inferred from the cirrus flow visible in the satellite observations and persisted for a number of days over the region of storm development. This upper divergence seemed to play a major role in the initial development of the storm.

The results of this study prove the usefulness of high resolution infrared and television observations from satellites for the investigation of small-scale phenomena as well as their interconnection with large-scale atmospheric processes in tropical meteorology.

CONTENTS


Abstract . . . . . ii

INTRODUCTION . . . . . 1

HIGH RESOLUTION INFRARED RADIOMETER DATA . . . . . 2

DEVELOPMENT OF TYPHOON MARIE AS DERIVED FROM SATELLITE OBSERVATIONS . . . . . 4

METEOROLOGICAL ASPECTS OF TYPHOON MARIE DEVELOPMENT . . . . . 6

APPARENT SIMILARITIES WITH THE DEVELOPMENT OF TYPHOON GILDA 1967 . . . . 12

CONCLUSIONS . . . . . 13

ACKNOWLEDGMENTS . . . . . 14

References . . . . . 14

APPENDICES—COMPILATION OF SATELLITE AND CONVENTIONAL OBSERVATIONS . . 17

Appendix A—October 24, 1966 . . . . . 19

Appendix B—October 25, 1966 . . . . . 27

Appendix C—October 26, 1966 . . . . . 35

Appendix D—October 27, 1966 . . . . . 43

Appendix E—October 28, 1966 . . . . . 51

Appendix F—October 29, 1966 . . . . . 59

Appendix G—October 30, 1966 . . . . . 65

Appendix H—October 31, 1966 . . . . . 71

Appendix I—November 1, 1966 . . . . . 77

Appendix J—November 2, 1966 . . . . . 83

Appendix K—November 3 through November 9, 1967 . . . . . 87

# A SATELLITE VIEW OF TYPHOON MARIE 1966 DEVELOPMENT

by
G. Warnecke* and L. J. Allison
*Goddard Space Flight Center*

E. R. Kreins, Major, USAF†
*USAF Environmental Technical Applications Center*

L. M. McMillin
*Allied Research Associates, Inc.*

## INTRODUCTION

In a comprehensive survey of problems in tropical meteorology, Alaka (1964) wrote the following on the broad-scale conditions of hurricane and typhoon development:

"It is a known fact that the incidence of hurricanes is directly related to atmospheric conditions beyond the immediate locality of the potential storm. Some of the known pertinent broad-scale features include the condition of the trades, the equatorward extension of the mid-latitude westerlies and the intensity and location of the subtropical highs and intertropical shearlines. The mechanism of the persistence and variations of these features and the nature and dynamics of their relation to hurricane formation and development need to be investigated."

This paper will demonstrate that satellite infrared and television observations can help in the investigation of these mechanisms and will present the results of a case study performed particularly for the early development stages of Typhoon Marie 1966 using high resolution observations of the Nimbus II and ESSA-3 meteorological satellites. In this connection, a complete documentation of the satellite observations of Typhoon Marie was achieved and is presented in the appendices of this report.

Satellite television pictures resemble normal photographs and need no explanation; however, introductory remarks are necessary to interpret the high resolution infrared radiometer (HRIR) data used in this report.

*On leave from the Free University of Berlin, Germany, as National Academy of Sciences–National Research Council Senior Postdoctoral Resident Research Associate with the National Aeronautics and Space Administration.
†Air Weather Service member temporarily attached to the Goddard Space Flight Center.

## HIGH RESOLUTION INFRARED RADIOMETER DATA

The Nimbus II high resolution infrared radiometer measured radiation in the 3.5- to 4.2-micron atmospheric "window" region. Detailed observations of three-dimensional cloud structures were made possible by the relatively small field of view of the instrument, which was 8.6 by 9.7 kilometers at the subsatellite point (determined by the average satellite altitude of 1100 kilometers and the 7.85 by 8.80 milliradians degree aperture of the instrument).

The radiometer measurements differ from satellite television pictures in that the infrared radiometer measures outgoing emitted radiation, while the television pictures depict differences in reflected solar radiation. In the 3.5- to 4.2-micron near-infrared region, only nighttime measurements detect pure thermal radiation. Atmospheric and terrestrial features are detected by daytime measurements also, but a separation of the two radiation components, and therefore a unique physical interpretation of the measurements in meteorological terms, is not possible because of the approximately equal radiances of the emitted thermal radiation and the near infrared reflected-solar radiation. In the absence of sunlight, blackbody radiation can be assumed and the detected radiance can be converted to the temperature of the radiating surface ("equivalent blackbody temperature," $T_{BB}$). This permits the derivation of earth or ocean surface temperatures, under clear sky conditions, and cloud top heights when an opaque, plane cloud surface fills the field of view of the radiometer. Examples of this technique and results from satellite experiments are well documented (NASA, 1965).

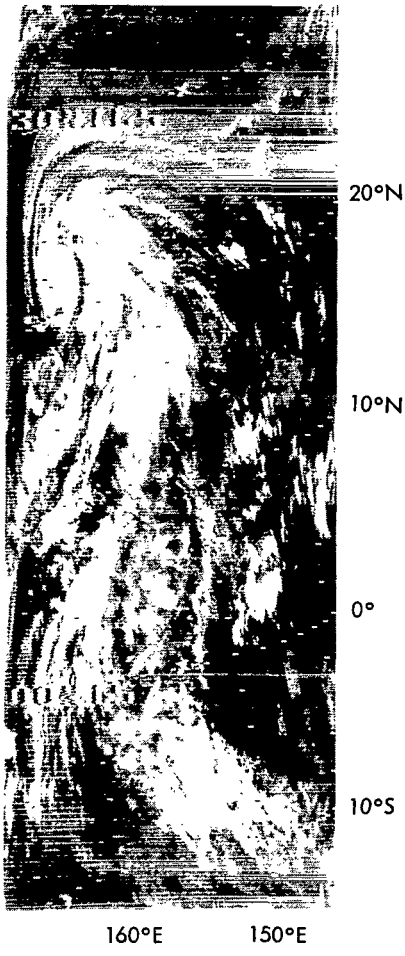


Figure 1—An example of photo imagery of Nimbus II HRIR data from orbit 2266 on November 1, 1966, showing Typhoon Marie near 20°N.

In the 3.5- to 4.2-micron range of the HRIR instrument, slight atmospheric attenuation by water vapor and carbon dioxide is still present and corrections of up to +5°K may have to be applied to the temperature maps. These corrections are directly proportional to the scan nadir angle and the variable atmospheric water vapor content.

The infrared data are presently available in two forms. One is a photographic image formed scan by scan from the original analog record of the data. This results in a pictorial view of the cloud and surface temperature structure. However, no absolute values of either temperatures or temperature differences can be derived from this display, because reproductions from the original negatives are exposure controlled. In addition, large distortions at the sides of the orbital strips prohibit a good mosaic of consecutive orbits. Nevertheless, the photo imagery has the advantage of being the more complete form of data display. An approximate geographic grid, accurate to within ±2 degrees of great circle arc at the subsatellite point, is superimposed upon the photographic image for a rough orientation. Figure 1 is an

example of an orbital film strip exhibiting the fully developed Typhoon Marie, the main subject of this study. The vortex center is marked by a cirrus canopy and no eye is discernible. The pronounced convective inflow spiral bands can be distinguished from the thinner and more diffuse cirrus outflow streamers. A large number of structural details can be seen in this photographic display, but the obvious distortions at the sides of the film-strip obscure part of the storm.

The second form of data, the grid print map, is a computer transformation of the data, calibrated in terms of equivalent blackbody temperature, into a standard geographical map projection (Mercator or polar stereographic) of various scales. The advantages of this form of presentation are the display of absolute values, the elimination of distortion, and the possibility of automatically composing measurements from consecutive orbits into quasi-synoptic areal maps. However, due to the scanning geometry, either a loss of detail will result from averaging in the center portions of each swath, or data gaps will occur at some distance from the subsatellite point where the data spacing is larger than the grid interval. Figure 2 is an example of a computer product showing the rectified composite of numerical data from three consecutive orbits, including the one of Figure 1, in a Mercator projection. Automatic contouring facilitates the recognition of patterns such as the large spiraling typhoon cloud system (center), the cloud band of the intertropical convergence zone (center right), and extratropical frontal cloud systems (upper left and lower right). The average minimum cloud top temperatures in the frontal cloud systems are around 230°K (approximately -40°C and corresponding to an average cloud top height of at least 11 kilometers). The lowest temperature shown over Typhoon Marie in this map is below 225°K, indicating cloud-top heights above 11.8 kilometers. Values colder than 230°K should, however, be viewed with some reservation because they are at the lower detection limits of the radiometer for this orbit.

The computer determines an average space view level from the measured space levels preceding and following each earth scan. All values within the earth scan that fall below this level are assigned a value of 190°K while higher values are assigned a temperature given by the calibration of the instrument. The space view or "noise equivalent temperature" for the case studied was around 230°K but varied with the cell temperature of the sensor. When a map is produced, these 190's are averaged with the other temperatures occurring within a given grid interval. Thus there is some uncertainty in all temperatures produced on such a map since 190's may be contained in the average of every grid point; but omitting the 190's from the map would not solve the problem because all the temperatures omitted would be below some level, thus causing the resulting averages to be too warm. The 190's are left on the maps because the resulting isopleths show at least the structure of the higher cloud systems. Also, all 190's that have been observed were in colder areas where high clouds were present. This means that, on such a map, high temperatures around 290°K are not likely to contain any 190's in the averages and are exact, while temperatures of 240°K may contain some 190's in the printed average value. Since the isotherms of values below the space view level which result on such a map obviously contain 190's in the averages, no temperature values are assigned to these lines in this area in the figures presented.

When interpreting the measured equivalent blackbody temperature as cloud-top temperature, an approximate conversion of these values into cloud top height can be performed using the tropical atmosphere of the 1966 U. S. Standard Atmosphere Supplements for the temperature-height relationship. This relationship is used in the legends of the second figure in each appendix.

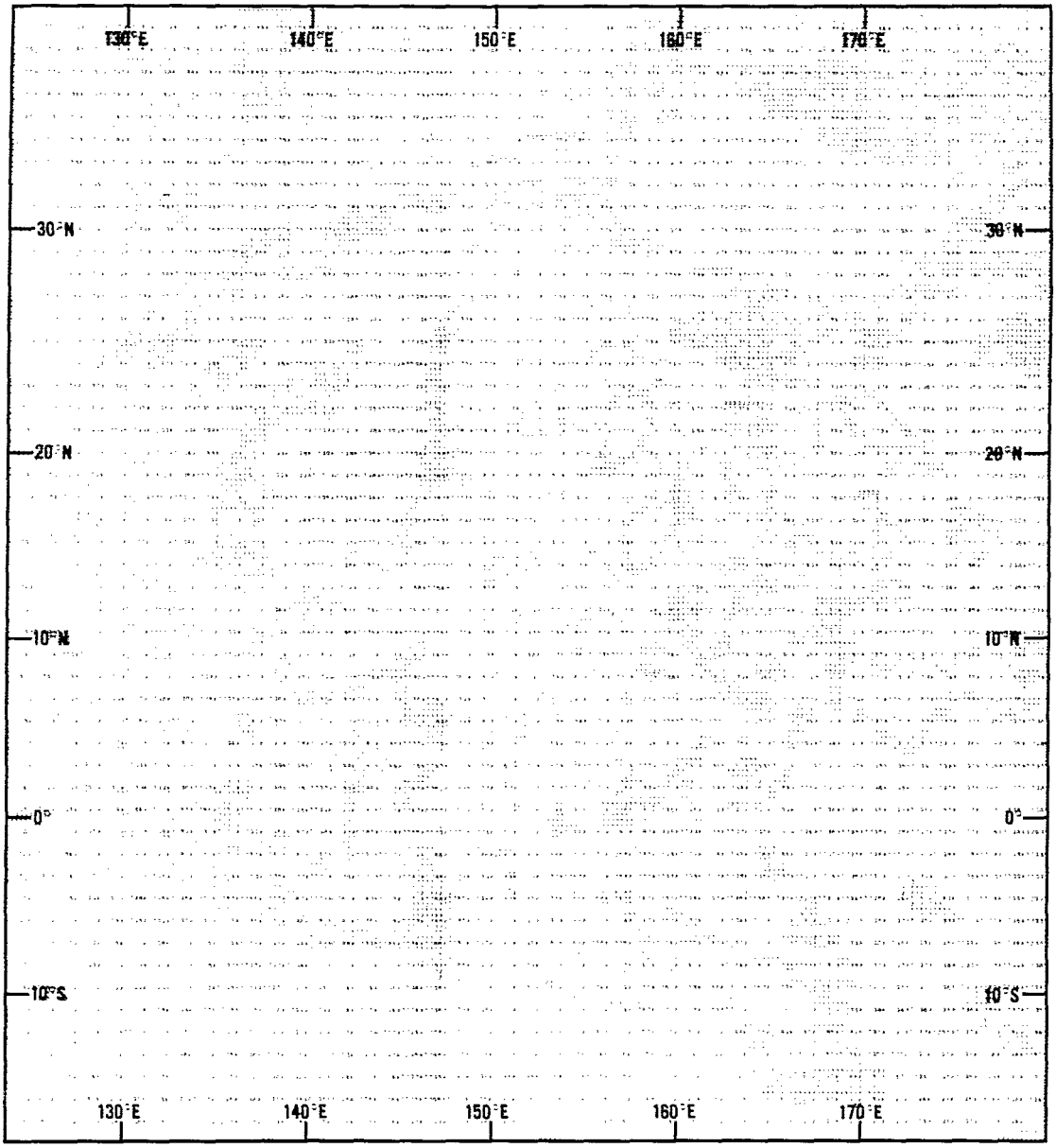


Figure 2—An example of a composite grid print map of Nimbus II HRIR data from orbits 2265, 2266, and 2267 on November 1, 1966. Projected on a Mercator Base (1 grid interval = 1.25 degrees longitude), showing Typhoon Marie near the center.

## DEVELOPMENT OF TYPHOON MARIE AS DERIVED FROM SATELLITE OBSERVATIONS

Typhoon Marie developed during the last ten days of October 1966 in an area bounded by 10°N., 20°N., 170°W., and 170°E.

On October 24, 1966, the remnants of a northern hemispheric extratropical frontal system are trailing into the development area producing a large number of cumulus clouds, which are organized

in some slightly curved cloud bands (Figure A4). The intertropical convergence (ITC) zone is weakly indicated in the cloud pattern of this region (Figures A1, A3). There seems to be an abrupt structural change in the ITC around 170°W. A continuous band of heavy, high-reaching cloudiness is associated with it east of this longitude, where one of the northern extratropical cloud bands merges into the ITC zone; west of this longitude the ITC appears poorly defined by the cloud pattern. The first indication of significant cloud development connected with the storm was found in this area on October 25, 1966.

Figure B1 is a montage of four HRIR film strips obtained from consecutive nighttime orbits on October 25, 1966. The most interesting feature in this figure is the boomerang-shaped cloud system composed of one northern and one southern hemispheric frontal cloud band, which join near the equator at 140°E. The ITC zone is indicated by the associated line of convective cloud systems between 5°N. and 10°N. The significant feature in the area of later storm development is a cluster of relatively small convective cloud systems. The different grey shades of these clouds on the original film strip indicate that the cloud tops vary in altitude. The apparent lack of cirrus anvils and the low radiation temperatures of some of them (indicating a high cloud top) suggest that a number of these clouds have developed into cumulonimbus calvus. The whole cluster appears to be unorganized because the smaller and lower clouds are too small to be resolved by the HRIR instrument.

However, because of the higher spatial resolution of the camera, the corresponding ESSA-3 photographs taken 12 hours earlier (Figures B3, and B4) show that a spiral formation existed within the same cloud cluster; but the photograph does not give any indication of the cloud-top heights. Obviously both techniques are useful and, when used together, provide a means for early detection of a convergent streamfield, at least at the lower tropospheric cloud level, and the build up of stronger convective cells within this area.

The analysis of a grid print map, reproduced as Figure B2, shows the HRIR measurements in a rectified version (Mercator map projection) for the night of October 25. The boomerang-shaped cloud system and the ITC cloud band stand out clearly. However, no structural details of the cloud cluster mentioned before are resolved because of the averaging of more than 200 measurements into one grid point of the grid print map. In the figure the cluster appears as a small isolated area of lower equivalent blackbody temperature indicated by the letter "M."

On the following day, October 26, the area in question is located at the boundary between two orbits from both the Nimbus II and ESSA-3 satellites and is so distorted on the photographic displays (Figures C1 and C3) that it is difficult to derive detailed characteristics of the particular cloud cluster. However, an intensification of a number of small convective cloud cells, some of which seem to have developed cirrus anvils, at least can be derived from the television picture; and the Nimbus II grid print map (Figure C2) confirms this by showing an expansion and intensification of the cold spot (M).

A drastic change occurred during the next 24 hours. On October 27, the HRIR grid print map (Figure D2) shows an extended high (cold) cloud system that seems to merge into the ITC zone of

cloudiness between 8°N. and 16°N. and 170°E. and 180° longitude. A detailed photograph of the HRIR data (Figure D1) reveals extended areas of high clouds, a pronounced spiral structure of these high reaching cloud systems, and a strong anticyclonic cirrus outflow. This outflow is suggested by the texture at the outer edges of the high-level spiral clouds. It should be emphasized that the main cirrus outflow occurs over and along the pronounced convective spiral cloud bands, while the center of the forming cyclone apparently shows areas of clear sky.

On the following day, October 28, the development of the cirrus shield of the storm seemed to cease temporarily, as indicated by higher equivalent blackbody temperatures in larger parts of the outflow bands (Figure E2) shown by the radiation measurements, although the television pictures seem to suggest the distinct organization of a solid, more symmetric vortex (Figures E3 and E4). In the afternoon of October 29, the storm shows the first indication of an eye near 15°N., 169°E. (Figures F3 and F4). According to Weather Bureau reports, the typhoon stage was reached on the next day, October 30, 1966. The HRIR photographs then show a pronounced cirrus canopy over the storm center and the eye is no longer visible on this day. The numerical analysis of the infrared data of November 1, 1966 (Figure I2), shows a large cirrus canopy above 11 kilometers, while the HRIR photograph shows the details of the inflow and outflow spirals (Figure I1). A striking feature in this case is the large scale outflow system at the cirrus level, which finally penetrates even into the southern hemisphere. This outflow can be located near the 200-mb level because, according to Johnson (1966), the cirrus flow seen in satellite pictures was repeatedly found to approximate the horizontal motion field at this level.

Regarding the cloud structure in the vicinity of the storm, an interesting phenomenon can be found in the presented catalog of pictures. During the early stages of development (October 27-29), the heaviest high-level outflow cloudiness was observed on the north and east side of the developing center. When the storm reached the typhoon stage (October 29-November 1), the main outflow cloudiness appeared on the southeast and south side of the vortex center with a very pronounced southwestward flow toward and across the equator. During the mature typhoon stage (November 2), when the storm approached an extratropical frontal system and began to assume a northeasterly course, it developed an extensive, high cloud system at its northern rim.

During the period of early development of Marie, another storm, Tropical Disturbance #34, started to develop at approximately 15 degrees longitude to the west. On October 30 it appeared to be almost as intense and as extensive as Marie. After this day, however, it rapidly decayed, while Marie reached typhoon stage. Finally on November 1 the remnants of this tropical disturbance were incorporated in the horizontally expanding flow system of Marie (Figures I1, I2, I3).

## METEOROLOGICAL ASPECTS OF TYPHOON MARIE DEVELOPMENT

The earliest indication of the development of Typhoon Marie was found, as mentioned earlier, in the satellite observations of October 25, 1966, close to 15°N. latitude and 180° longitude, an area with no weather station closer than 1200 kilometers. The physical state of the troposphere in this region can be obtained only by interpolation of conventional data and inference from the satellite observations.

The development of Marie as seen in the satellite data described in the previous section, and more extensively treated by Fett (1968) and also briefly discussed before by Warnecke et al. (1968), seems to follow the lines of tropical storm development as recently surveyed by Gray (1967), with the exception of his stated opinion on the negligible importance of upper tropospheric (perhaps 200 mb) divergence for the *initial* tropical storm development. Gray's list of necessary conditions for tropical storm development is fulfilled in this case. The distance of the development area from the ITC cloud band located at 7°N. to 8°N. in the satellite observations (Figures B1 and B3) was found to be 7° to 8°. This ITC cloud band was assumed to coincide with Gray's equatorial surface pressure trough, which could not be located accurately with the sparse conventional data available. The development occurred over water warmer than 26.5°C (79.7°F), since ocean surface temperatures of at least 28°C were detected by the HRIR sensor. This is consistent with the climatological mean temperature for October (Figure 3). The large-scale general low level flow was convergent (Figure 6). The vertical zonal wind shear was very weak in this region, as shown in Table 1.

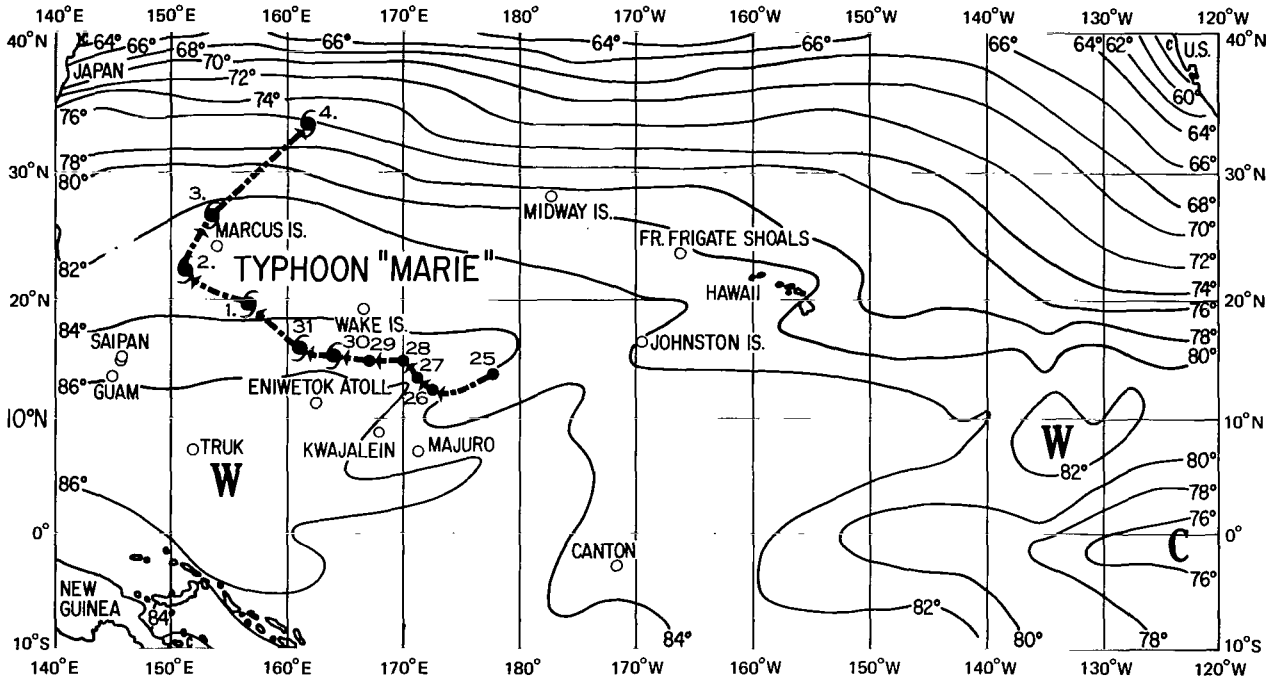


Figure 3—Monthly mean sea surface temperature (°F.) of the Pacific Ocean for October (from U. S. Naval Oceanographic Office, 1968) and track of Typhoon Marie from October 25 through November 4, 1966.

Table 2, which lists radiosonde measurements at the nearest stations, shows that this situation was persistent for several days. A deep layer of high relative humidity existed in the lower troposphere, since, according to Table 2, the top of the moist layer is in the vicinity of the 700- and 800-mb levels or 2000 to 3000 m, respectively. Thus the reservoir of latent heat is fairly large; the tropospheric total precipitable water content computed from the radiosonde data over Wake Island on October 24, 1966 was 4.0 cm.

Table 1

Wind at 15°N., 180°W. on October 24, 1966 1200 GMT
(by Horizontal Interpolation from Surrounding Observations).

| Atmospheric Pressure (mb) | Wind | |
|---|---|---|
| | (deg) | (mps) |
| 200 | 360 | 5 |
| 500 | 080 | 8 |
| 700 | 090 | 10 |
| Surface | 080 | 8 |

The time-sections of radiosonde observations over Wake Island, and Eniwetok Atoll, Marshall Islands (Figures 4 and 5), characterize the upper air conditions at some distance from the typhoon. These were the two stations the storm most closely approached when it passed halfway between them around October 30, 1966 (compare Figure 3) as a mature typhoon. Over Wake Island, only intensified easterlies were observed below 300 mb. The winds at the 200- and 150-mb levels, however, responded clearly to the anticyclonic, high-level outflow observed in the satellite observations. Over Eniwetok Atoll (Figure 5), located south of the typhoon track, the lower tropospheric winds showed the storm passage by shifting to westerly directions, while the upper tropospheric winds between 300 mb and 150 mb indicated the anticyclonic outflow.

The synoptic situation over the central Pacific during the period of time considered is illustrated by a surface weather map and a series of 200-mb streamline maps which were constructed in order to investigate the dynamics of Typhoon Marie development. The synoptic surface analysis of October 24, 1966, 1200 GMT (Figure 6) is based on conventional surface observations and the presented satellite television and infrared data (Appendix A). The extensions of the mid-latitude frontal cloud bands, which are so obvious in the satellite observations, are identified by open circles along a solid line and are usually in good agreement with surface cloud observations. Conventional trough lines are marked by dashed lines, and the ITC zone is delineated by a dashed double-line. Its position is mainly based on satellite information.

The 200-mb streamline patterns were constructed from 200-mb radiosonde wind observations and wind directions derived from cirrus blown off in distinct cloud bands from the high-reaching convective cloud systems (Jager et al. 1968), as seen in the satellite observations (Appendices A to E).

The large-scale synoptic situation is characterized by the approach of the remnants of a southern and a northern hemispheric extratropical frontal cloud system into the equatorial region. These frontal remnants can be identified only by their cloud bands as seen in satellite television pictures and infrared photo imagery, as well as upper tropospheric (200-mb level) troughs, rather than by conventional surface observations. Although the lower tropospheric portions of these former fronts dissipated when passing through the subtropics, the upper tropospheric cloud-producing or rather cloud-maintaining processes seem to survive and are thus reflected in the cloud features described.

In detail, the cloud photographs on October 24, 1966, the day before any obvious indication of the later storm development was present (Appendix A), show a widely unorganized cumulus convection pattern around 15°N. and 180°W. This cumulus convection was activated by the intrusion into this area of the slowly southward moving remnants of a former cold front (Figure 6), still

Table 2

Radiosonde Measurements in the Vicinity of the Typhoon Marie Early Development Area.

| Atmos. Press. (mb) | October 22, 1966; 00 GMT | | | | | | | | | | | | October 23, 1966; 00 GMT | | | | | | | | | | | | October 24, 1966; 00 GMT | | | | | | | | | | | |
|---|---|---|---|---|---|---|---|---|---|---|---|---|---|---|---|---|---|---|---|---|---|---|---|---|---|---|---|---|---|---|---|---|---|---|---|---|
| | Johnston Island | | | | Wake Island | | | | Majuro Island | | | | Johnston Island | | | | Wake Island | | | | Majuro Island | | | | Johnston Island | | | | Wake Island | | | | Majuro Island | | | |
| | Temp | R.H. | Wind deg | Wind mps | Temp | R.H. | Wind deg | Wind mps | Temp | R.H. | Wind deg | Wind mps | Temp | R.H. | Wind deg | Wind mps | Temp | R.H. | Wind deg | Wind mps | Temp | R.H. | Wind deg | Wind mps | Temp | R.H. | Wind deg | Wind mps | Temp | R.H. | Wind deg | Wind mps | Temp | R.H. | Wind deg | Wind mps |
| 200 | -53 | — | 182 | 10 | -53 | — | 130 | 03 | -53 | — | 216 | 09 | -53 | — | 276 | 10 | -53 | — | 005 | 04 | -53 | — | 300 | 11 | -52 | — | 264 | 13 | -53 | — | 355 | 08 | -52 | — | 290 | 05 |
| 300 | -33 | 53 | 219 | 15 | -32 | 18 | 050 | 03 | -30 | 20 | 099 | 07 | -32 | 24 | 260 | 17 | -32 | 16 | 161 | 04 | -30 | 19 | 115 | 06 | -31 | 14 | 255 | 15 | -32 | 18 | 326 | 02 | -30 | 27 | 115 | 05 |
| 400 | -17 | 33 | 233 | 10 | -18 | 18 | 059 | 16 | -15 | 27 | 104 | 06 | -16 | 25 | 259 | 14 | -17 | 16 | 106 | 12 | -15 | 36 | 080 | 08 | -17 | 19 | 236 | 05 | -16 | 17 | 147 | 02 | -15 | 31 | 124 | 04 |
| 500 | - 6 | 60 | 244 | 06 | - 5 | 17 | 082 | 10 | - 6 | 53 | 089 | 06 | - 6 | 33 | 260 | 06 | - 6 | 15 | 090 | 13 | - 5 | 16 | 106 | 12 | - 8 | 45 | 062 | 07 | - 5 | 17 | 139 | 10 | - 4 | 19 | 128 | 05 |
| 700 | 9 | 78 | 098 | 03 | 10 | 70 | 104 | 07 | 11 | 33 | 109 | 11 | 11 | 39 | 029 | 04 | 10 | 56 | 091 | 08 | 11 | 32 | 094 | 09 | 9 | 57 | 077 | 16 | 11 | 19 | 104 | 09 | 10 | 49 | 084 | 14 |
| 800 | 15 | 76 | 083 | 05 | 15 | 71 | 093 | 08 | 16 | 30 | 108 | 09 | 17 | 53 | 044 | 07 | 16 | 61 | 107 | 07 | 15 | 69 | 088 | 08 | 14 | 65 | 076 | 12 | 16 | 67 | 097 | 08 | 15 | 67 | 067 | 08 |
| 850 | 18 | 63 | 065 | 07 | 17 | 78 | 093 | 11 | 18 | 41 | 105 | 10 | 19 | 63 | 300 | 03 | 18 | 67 | 110 | 07 | 18 | 62 | 100 | 08 | 18 | 68 | 075 | 14 | 18 | 76 | 088 | 11 | 18 | 74 | 078 | 08 |
| 900 | 21 | 61 | 060 | 08 | 19 | 85 | 087 | 13 | 21 | 59 | 100 | 10 | 21 | 72 | 056 | 08 | 20 | 74 | 114 | 08 | 20 | 66 | 103 | 09 | 21 | 66 | 078 | 12 | 21 | 65 | 089 | 11 | 21 | 73 | 091 | 07 |
| 950 | 23 | 75 | 056 | 11 | 22 | 80 | 079 | 13 | 23 | 74 | 092 | 08 | 23 | 71 | 060 | 09 | 23 | 72 | 094 | 08 | 23 | 69 | 117 | 05 | 22 | 72 | 082 | 12 | 24 | 84 | 084 | 11 | 24 | 82 | 078 | 05 |
| 1000 | 25 | 88 | 074 | 11 | 26 | 83 | 050 | 11 | 29 | 69 | 085 | 06 | 28 | 75 | 058 | 07 | 27 | 75 | 074 | 08 | 28 | 68 | 122 | 04 | 25 | 79 | 086 | 10 | 27 | 84 | 062 | 10 | 28 | 75 | 069 | 05 |
| SFC | 25 | 91 | 080 | 10 | 28 | 87 | 040 | 10 | 30 | 73 | 080 | 05 | 29 | 78 | 060 | 07 | 29 | 82 | 060 | 06 | 30 | 71 | 120 | 03 | 27 | 80 | 090 | 08 | 28 | 84 | 050 | 09 | 29 | 75 | 070 | 05 |

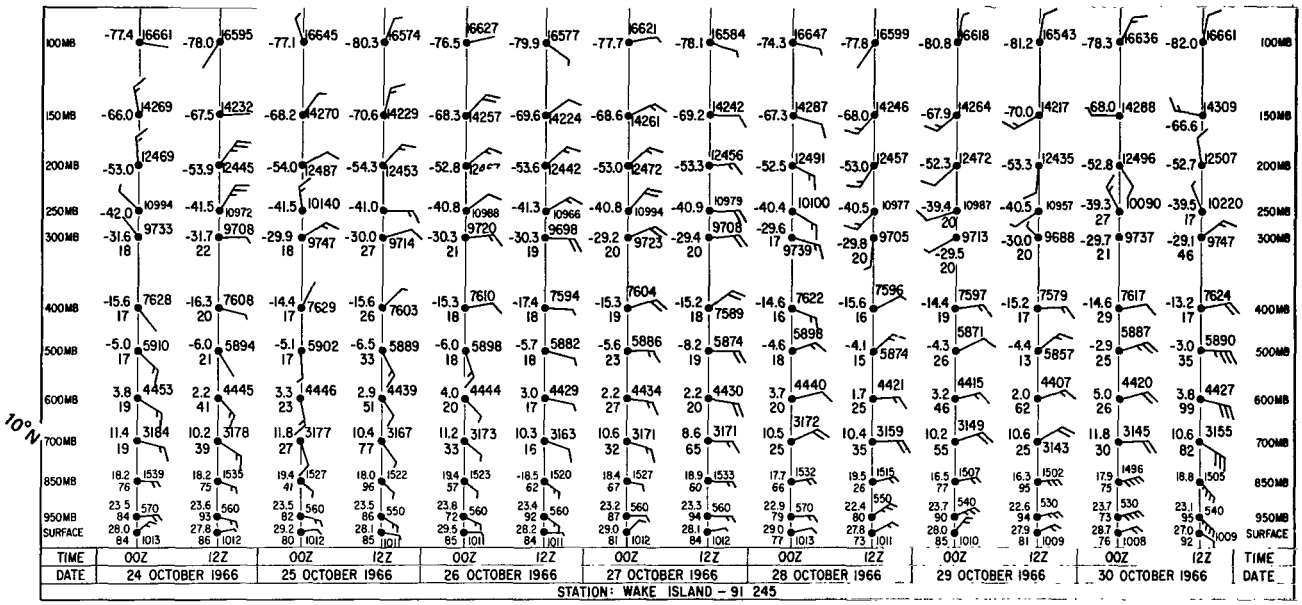


Figure 4—Time-section of radiosonde observations from October 24 to October 30, 1966, over Wake Island (19°N., 167°E.), indicating temperature (°C.), altitude (gpm), relative humidity (%), and wind (degrees; a full barb equals 10 knots) at standard pressure levels.

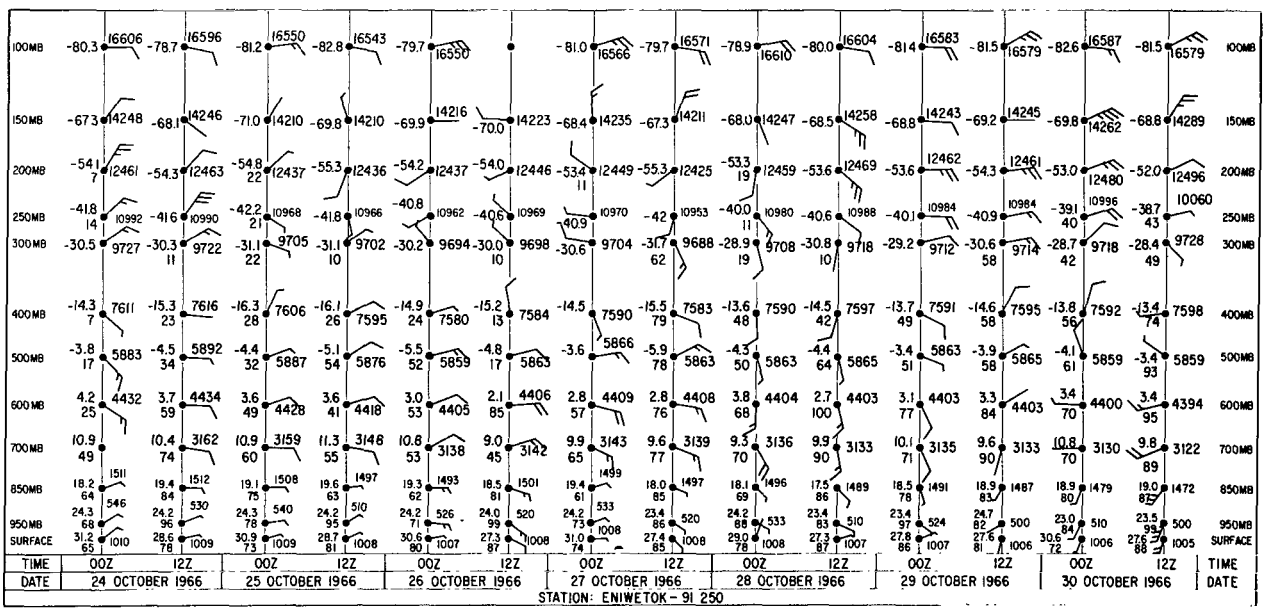


Figure 5—Time-section of radiosonde observations from October 24 to October 30, 1966, over Eniwetok Atoll (11°N., 162°E.), indicating temperature (°C.), altitude (gpm), relative humidity (%), and wind (degrees; a full barb equals 10 knots) at standard pressure levels.

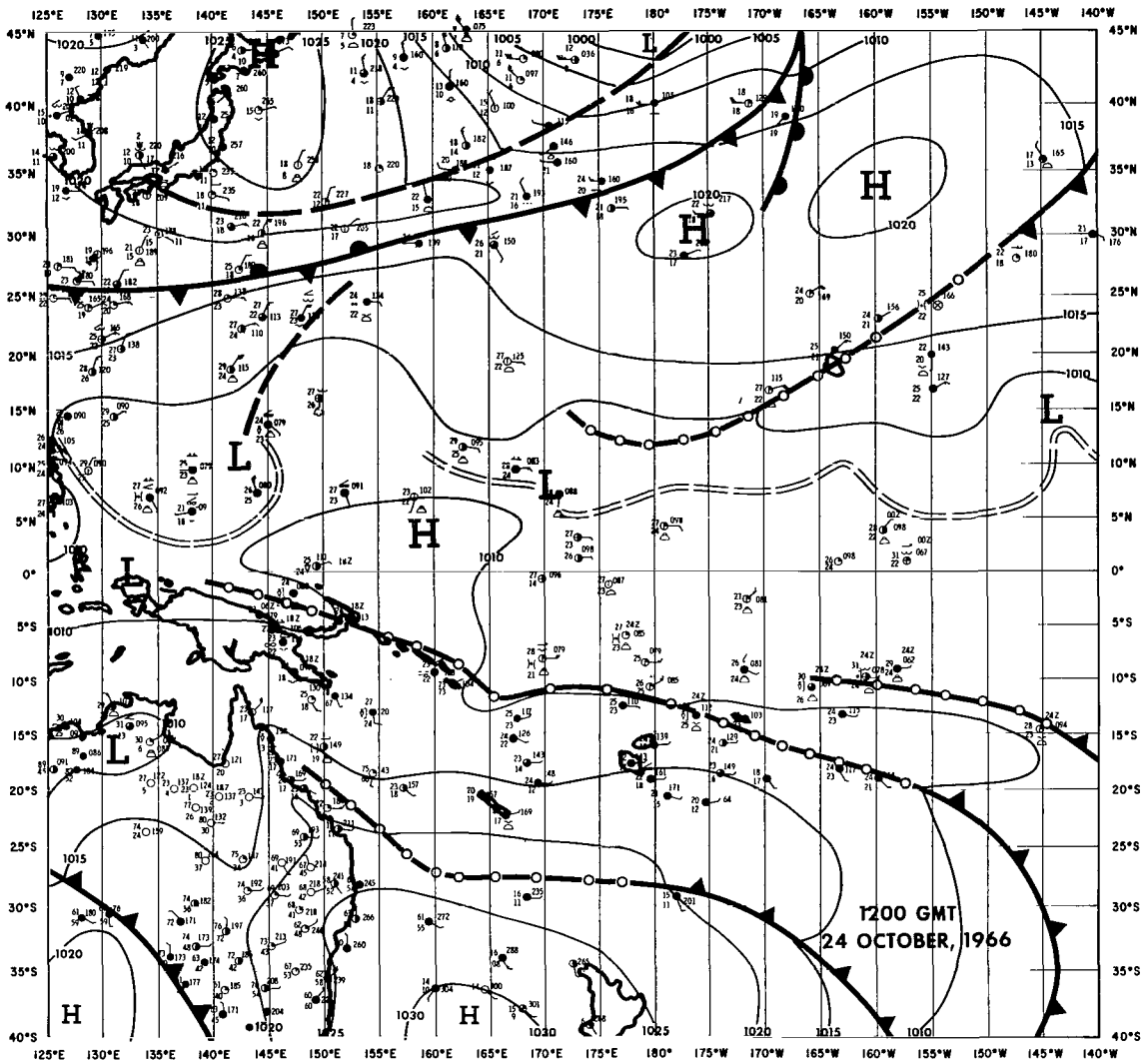


Figure 6—Surface weather map over the eastern central Pacific Ocean (October 24, 1966, 1200 GMT).

recognizable in the television and infrared cloud pictures and associated with a 200-mb streamline trough (Figure A5). In front of this trough, a streamline divergence can be observed, particularly near its southwestern-most extremities. This streamline divergence was rather persistent during the period of early storm development and over the region where the development took place (Figures A5 through E5). It is this dynamic feature that convinced the authors that high-level divergence is an important factor for the initial tropical storm development, at least in this case of Typhoon Marie. As mentioned above, this is contrary to Gray's statement. In this case of October 1966, a second perturbation (Tropical Disturbance #34) was generated nearby under the same upper flow pattern approximately 15 degrees of longitude to the west of Marie. This disturbance developed its own anticyclonic 200-mb vortex before the development of Marie's anticyclonic circulation (Figures C5 and D5). However, it rapidly disappeared on October 28. At the same time the

pre-existing anticyclonic vortex in front of the next 200-mb trough approaching from the northwest moved over the developing storm Marie and consequently accelerated its development into a full-grown typhoon while #34 decayed.

The cirrus flow visible in the satellite pictures actually is indicating flow direction only and thus shows diffluence rather than divergence. A correlation between true horizontal divergence and cirrus cloud patterns has not been established yet because of a number of obvious difficulties (Johnson, 1966). However, from the cloud development seen in the satellite pictures in this case, it seems very unlikely that the velocity distribution in the rapidly expanding cirrus bands would compensate for the observed diffluence to the extent that no net horizontal divergence would result. Pronounced streamline divergence, in this sense, strongly suggests that wind divergence was found to persist for days over the development area, not only during the latter stages of the typhoon but also during the very early stages of detectable development as can be seen in Figures A5 through E5. In addition, the 200-mb streamline analyses suggest a coupling between the storm development and the mid-Pacific trough, as described by Sadler (1963 and 1967), since the tropical storm development occurred near the extreme southwestern tip of this trough. The mid-Pacific trough originally introduced as a climatological upper tropospheric feature (Dean, 1956) should be interpreted, however, as the result of sequences of extratropical fronts penetrating the subtropics and finally stalling in this particular area. This means that the divergence pattern in the upper tropospheric streamfield undergoes a continuous cycle of appearance and decay, and the maximum of the resulting divergence will depend on the respective strength and structure of each individual frontal system. A corresponding region where extratropical frontal disturbances penetrate the subtropics and stagnate is found in the South Pacific in the same longitudinal area, as seen in TIROS VII radiation data (Allison et al., 1968).

In this particular case, it seems that the divergence of the anticyclonic flow (Figures A5 to E5) north of the almost zonally oriented mid-Pacific trough is particularly strong because of the next approaching mid-latitude frontal system. This results in stronger dynamic effects in the trough region. The high-level diffluence south of the trough seems also to be intensified, at least partly, by two southern hemispheric troughs approaching the same region in phase with the northern hemispheric systems and thus forming the boomerang-shaped, large-scale cloud configuration mentioned before.

A similar case of typhoon development (Gilda and Annie, 1967) one year later, as described in the following section, supports the conclusion that this configuration of cloud bands which represent the remnants of former mid-latitude frontal systems should be considered an essential factor in the Typhoon Marie development.

## APPARENT SIMILARITIES WITH THE DEVELOPMENT OF TYPHOON GILDA 1967

The early development stages of Typhoons Marie 1966 and Gilda 1967 appear to have been very similar. The cloud pattern, previous to the Gilda development, on November 4, 1967 at 5°N. to 10°N. and 175°E. to 170°W. (Figure K2) was similar to the pattern observed for Marie on October 27, 1966

between 12°N. and 16°N. and 167°E. and 180°E. In both cases, the ITC in this area was shown by the satellite pictures to be intense with long cirrus streamers blowing toward the east. These streamers showed a strong streamline divergence indicative of horizontal mass divergence. In both cases the later storm development occurred somewhat to the west of this cloud feature.

Similarity also existed in the large-scale cloud features such as the boomerang-like cloud pattern that was observed previously to the storm formation. This pronounced cloud pattern exhibited on November 3, 1967 (Figure K1) was formed by a cloud band, north of Australia, which extended from 13°S. at 170°W. to 10°S. at 155°E. and intersected the equator near 135°E., together with a frontal cloud band in the northern hemisphere which extended from 40°N. at 168°W. to 30°N. at 180°W. and continued to 25°N. at 165°E. The connection between the frontal cloud band and the ITC was not as strong as observed in the Marie case, but an indication of a heavier cloud mass is present around 155°E. Near the area of later storm development, at 3°N. and 160 to 165°E., some small cumuliform clouds are seen, as was observed in the 1966 case.

On November 4, 1967 (Figure K2), the pattern formed by the cloud bands in the southern hemipshere was essentially unchanged. The cold front in the northerm hemisphere extended from 145°E. at 30°N. to 155°E. at 35°N. and continued northeastward to a low center located off the Oregon coast. The ITC from 160°E. to 170°E. appears as a number of small intense cumulus cells.

On November 5 (Figure K3), a number of small cumulus cells appear near 0° to 3°N. and 163° to 168°E. One day later (November 6, Figure K4), the organized cirrus outflow of a developing system can be seen centered at 2°N. and 164°E. The full typhoon stage of Gilda was reached on November 7 (Figure K5), and, while a very strong upper outflow southward across the equator was visible on November 8, the rare case of a twin storm development rapidly occurred south of Gilda at 5°S. (Figure K6), with Typhoon Annie 1967 fully developed on November 9 (Figure K7).

## CONCLUSIONS

One of the most significant advantages of remote sensing techniques from a quasipolar orbiting satellite is the ability to produce global maps of the observed quantities. In this way, a wealth of meteorological information can be obtained from such large data-sparse areas as the eastern and central Pacific Ocean. In this study the meteorological conditions over the mid-Pacific Ocean were investigated for part of the 1966 typhoon season. Twelve-hour continuity was provided by the nighttime Nimbus II HRIR observations and the daytime ESSA-3 satellite television pictures. This information was used in combination with the limited conventional meteorological data to derive upper and lower tropospheric streamfields and to study the interaction of extratropical disturbances of both hemispheres with the intertropical circulation before and during the development of Typhoon Marie 1966.

The development of this typhoon could be followed from the earliest stage of an organized circulation pattern in low-level cumulus around 15°N. and 180° longitude through the growth of the convection cloud into cumulonimbus, through the development of cirrus anvils and a cirrus canopy,

to the final, full typhoon stage. The development took place in the tropical Pacific where the following conditions existed: surface water warmer than 28°C, high water vapor content in the lower troposphere, low-level wind convergence, weak vertical wind shear, and the area located 7° to 8° latitude north of the equatorial trough. The development also took place close to an area where the remnants of extratropical frontal disturbances, characterized by 200-mb troughs and distinct cloud bands, approached the ITC zone from both hemispheres. Upper tropospheric (200-mb) streamline maps constructed from radiosonde observations, as well as satellite pictures (cirrus flow), indicated persistent upper divergence over the development area in connection with these troughs. These seemed to play an essential role in the storm development.

With the present description of the development history of Typhoons Marie 1966 and Gilda 1967, and particularly the emphasis on the influence of the former mid-latitude frontal disturbances on the divergence pattern over the development area, the authors do not intend to suggest that this kind of development is the only or even the main cause of tropical storm development; rather, in the investigated case, the described mechanisms seem to have worked. This interaction between the extratropical and tropical circulations certainly is only one of several ways a tropical storm may develop. Stronger upper-tropospheric divergence, intensifying the pre-existing surface convergence and the consequently continuous and widespread convective heat release, may occur under a number of configurations of meteorological systems other than the one discussed here. More cases must be studied to cover the full spectrum of possible conditions. Satellite infrared and television data from near-earth orbits are, as was found, already very useful diagnostic tools for tropical meteorological research. Future use of similar observations, as well as observations from geosynchronous satellites should provide an even better insight into tropical circulation phenomena.

## ACKNOWLEDGMENTS

The authors wish to thank Mr. William R. Bandeen, Goddard Space Flight Center, for his helpful comments and suggestions in the review of this paper. We are particularly grateful to the National Environmental Satellite Center, ESSA, for providing the ESSA-3 satellite television data used in this study.

Goddard Space Flight Center
National Aeronautics and Space Administration
Greenbelt, Maryland, May 7, 1968
160-44-03-96-51

## REFERENCES

Alaka, M. A., 1964: "Problems of Tropical Meteorology: a Survey," Technical Note No. 62, Geneva: World Meteorological Organization.

Allison, L. J., Kreins, E. R., Godshall, F. A., and Warnecke, G., 1968: "Monthly Global Circulation Characteristics as Reflected in TIROS VII Radiometric Measurements," NASA Goddard Space Flight Center, Technical Note. (In preparation)

Dean, G. A., 1956: "The 1955 Mean Monthly Wind Circulation Over the Tropical Central Pacific Area," Paper No. 2, Contract No. AF 19 (604)-546, Los Angeles: Institute of Geophysics, University of California.

ESSA, Environmental Data Service, "Catalog of Meteorological Satellite Data, ESSA-3 Television Cloud Photography," Part I, 1968.

Fett, R. W., 1968: "Typhoon Formation Within the Zone of the ITC," *Monthly Weather Review* 96(2):106-117.

Gray, W. M., 1967: "Global View of the Origin of Tropical Disturbances and Storms," Atmospheric Science Paper No. 114, Fort Collins, Col.: Department of Atmospheric Science, Colorado State University.

Jager, G., Follansbee, W. A., and Oliver, V. J., 1968: "Operational Utilization of Upper Tropospheric Wind Estimates Based on Meteorological Satellite Photographs," National Environmental Satellite Center Technical Memorandum NESCTM-8, Washington, D. C.

Johnson, H. M., 1966: "Motions in the Upper Troposphere as Revealed by Satellite-Observed Cirrus Formations," ESSA Technical Report NESC-39, Washington, D. C.: Environmental Science Services Administration, National Environmental Satellite Center.

National Aeronautics and Space Administration, 1965: "Observations from the Nimbus I Meteorological Satellite," NASA Special Publication-89, Washington, D. C.

Sadler, J. M., 1963: "Utilization of Meteorological Satellite Cloud Data in Tropical Meteorology," *Proceedings of the First International Symposium on Rocket and Satellite Meteorology*, Amsterdam: North-Holland Publishing Company, pp. 333-356.

Sadler, J. M., 1967: "The Tropical Upper Tropospheric Trough as a Secondary Source of Typhoons and a Primary Source of Tradewind Disturbances," Final Report HIG-67-12, Contract No. AF 19 (628)-3860, Honolulu: Hawaii Institute of Geophysics, University of Hawaii.

U. S. Naval Oceanographic Office, 1968: "Monthly Charts of Mean, Minimum, and Maximum Sea Surface Temperature in the Pacific Ocean," Informal Report IR No. 68-2, Washington, D. C.

Warnecke, G., Allison, L. J., Kreins, E. R., and McMillin, L. M., 1968: "The Development of Typhoon 'Marie 1966' as revealed by Nimbus II High Resolution Infrared and ESSA-3 Television Data," *Proceedings of the Fifth Technical Conference on Hurricanes and Tropical Meteorology*, Caracas, Venezuela (in print).

Appendices

# COMPILATION OF SATELLITE AND CONVENTIONAL OBSERVATIONS

Appendix A

## October 24, 1966

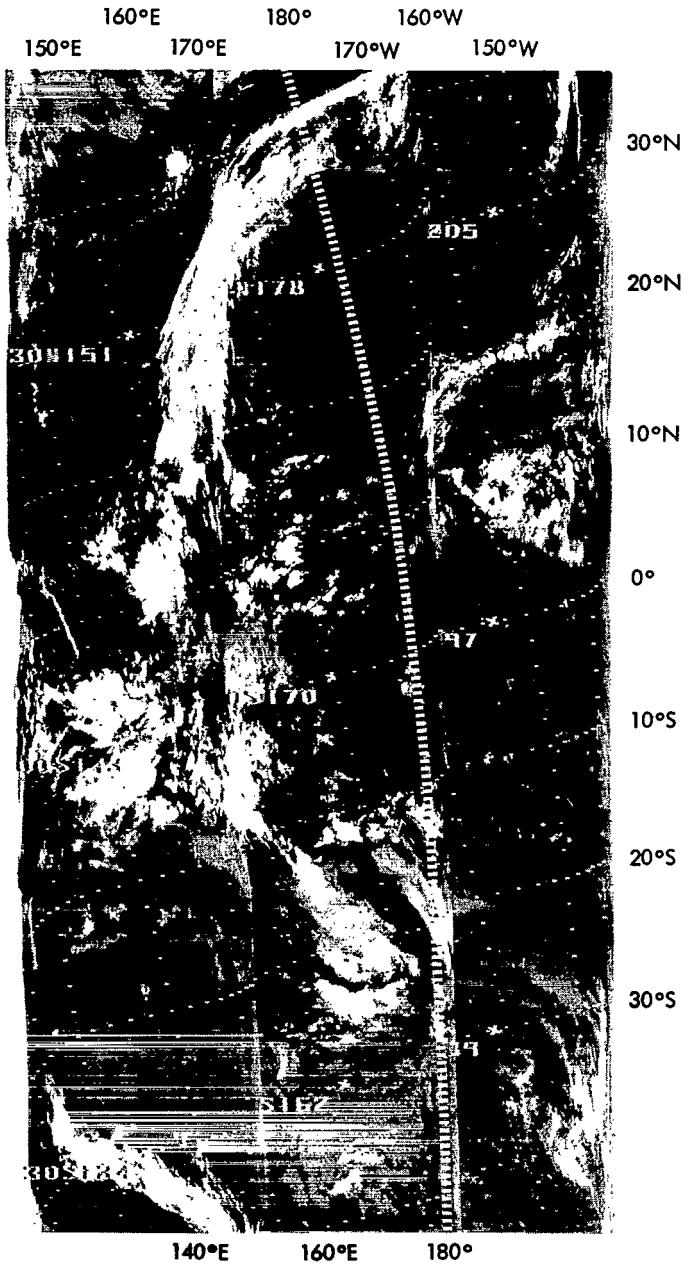


Figure A1—Montage of Nimbus II HRIR filmstrips (orbits 2158, 2159, and 2160) on October 24, 1966, 1200 GMT (near local midnight). The dashed line is the 180° meridian.

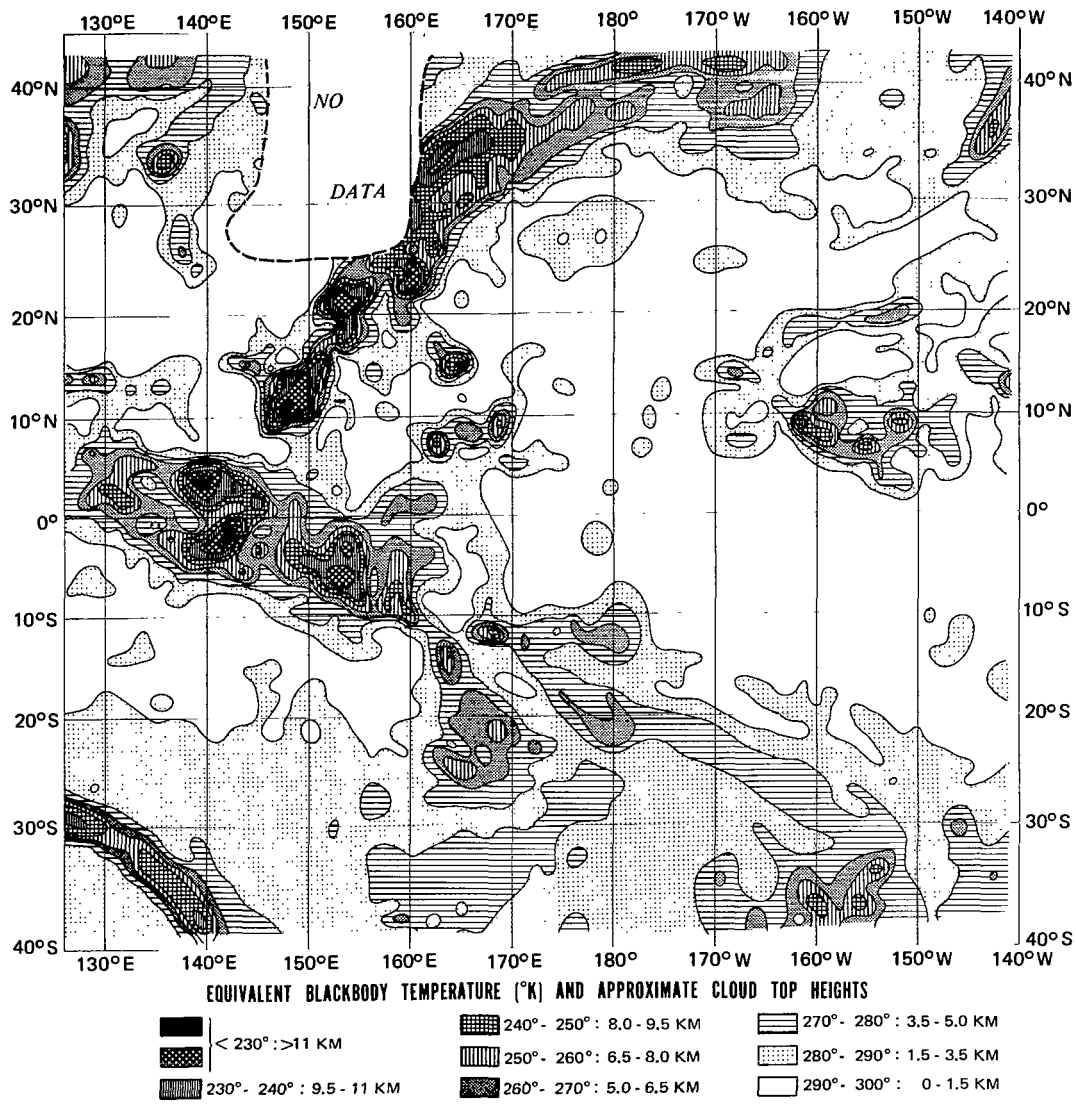


Figure A2—Analysis of Nimbus II HRIR measurements (orbits 2157, 2158, 2159, 2160, and 2161) on October 24, 1966, 1200 GMT (near local midnight) based on a computer grid print map with 1.25 degrees longitude per grid interval.

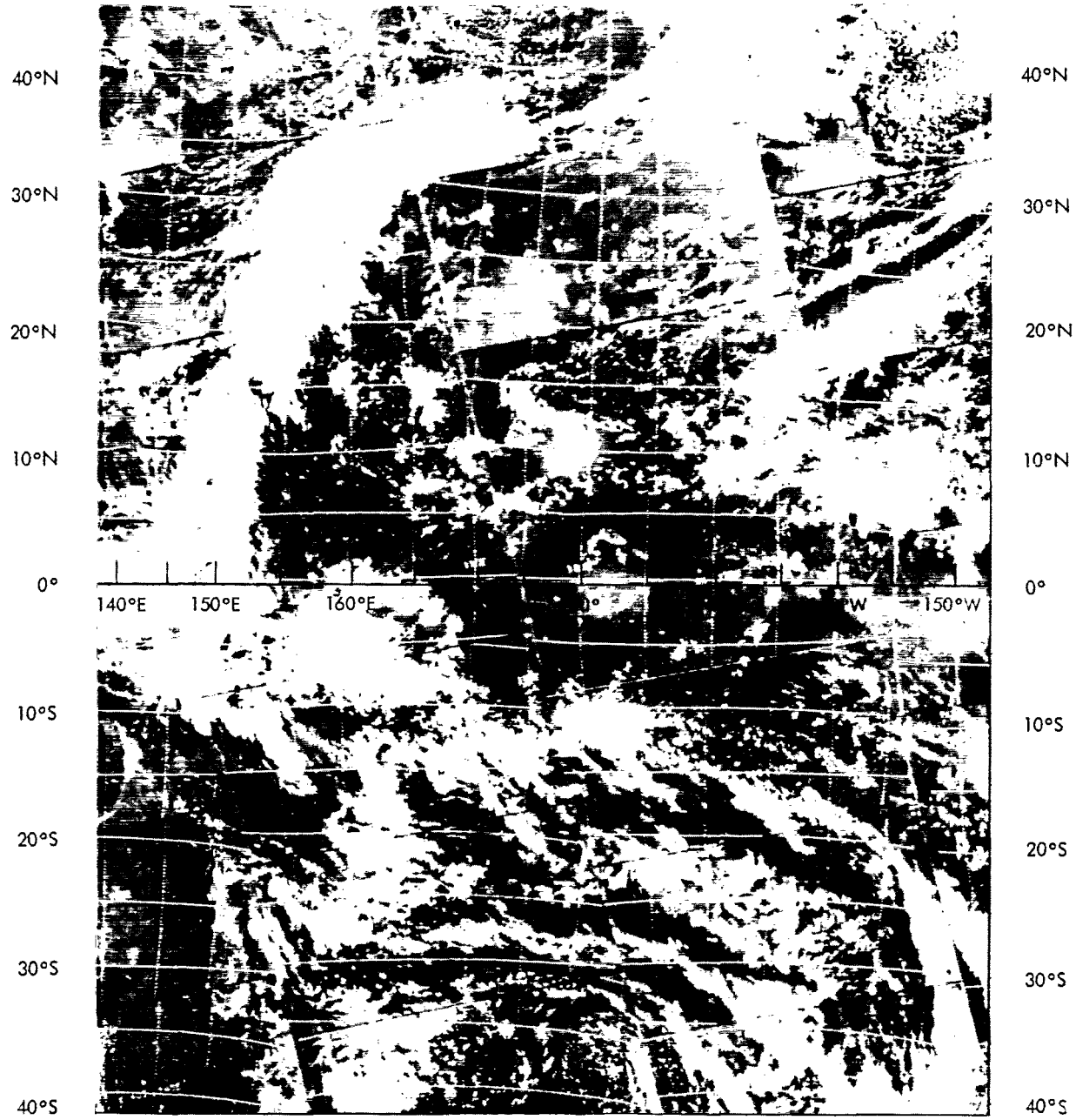


Figure A3—Montage of ESSA-3 television photographs (orbits 270, 271, 272, and 273) on October 24, 1966, near 0200 GMT (local early afternoon).

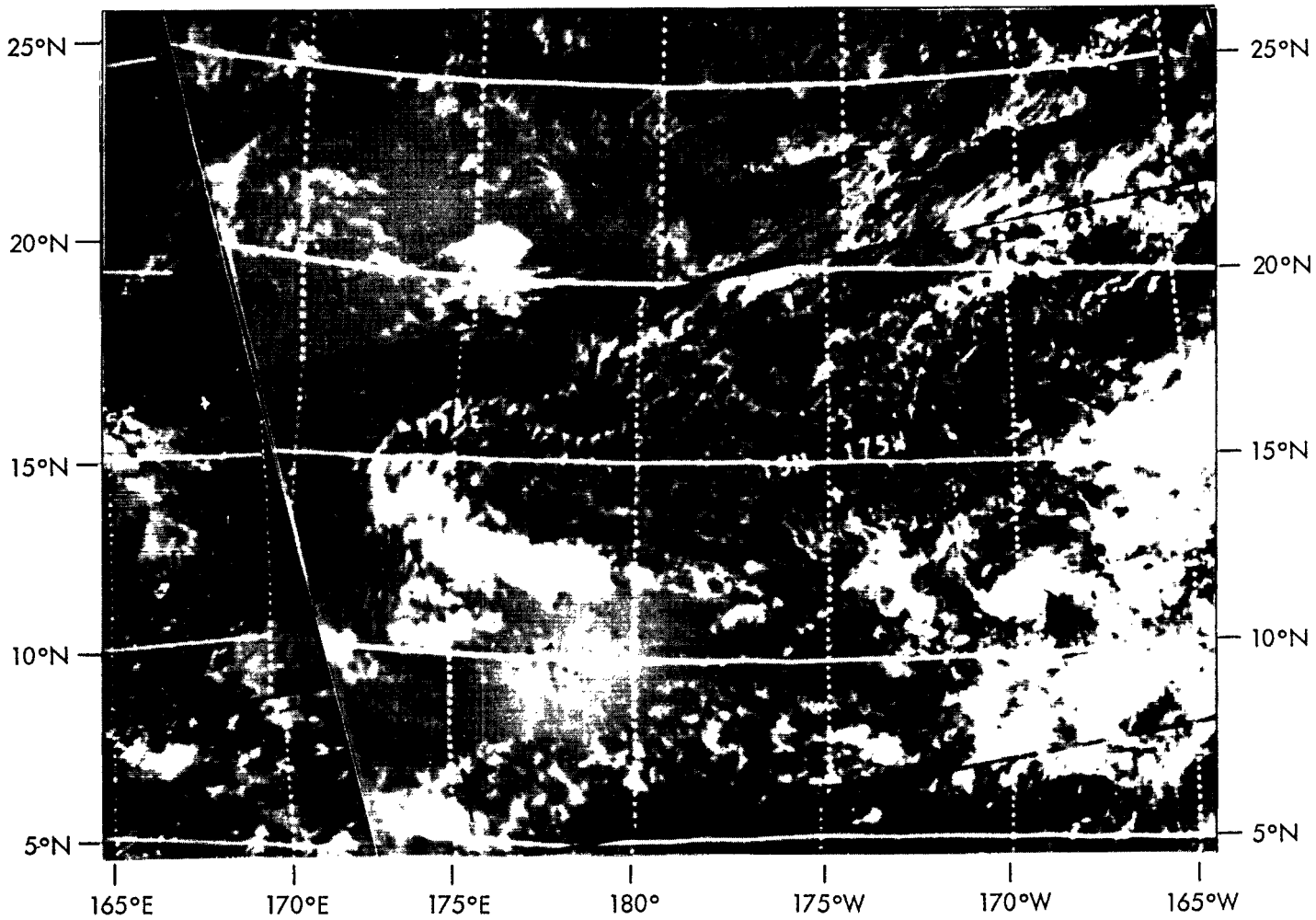


Figure A4—Montage of ESSA-3 television photographs (orbits 271 and 272) on October 24, 1966, near 0200 GMT (local early afternoon).

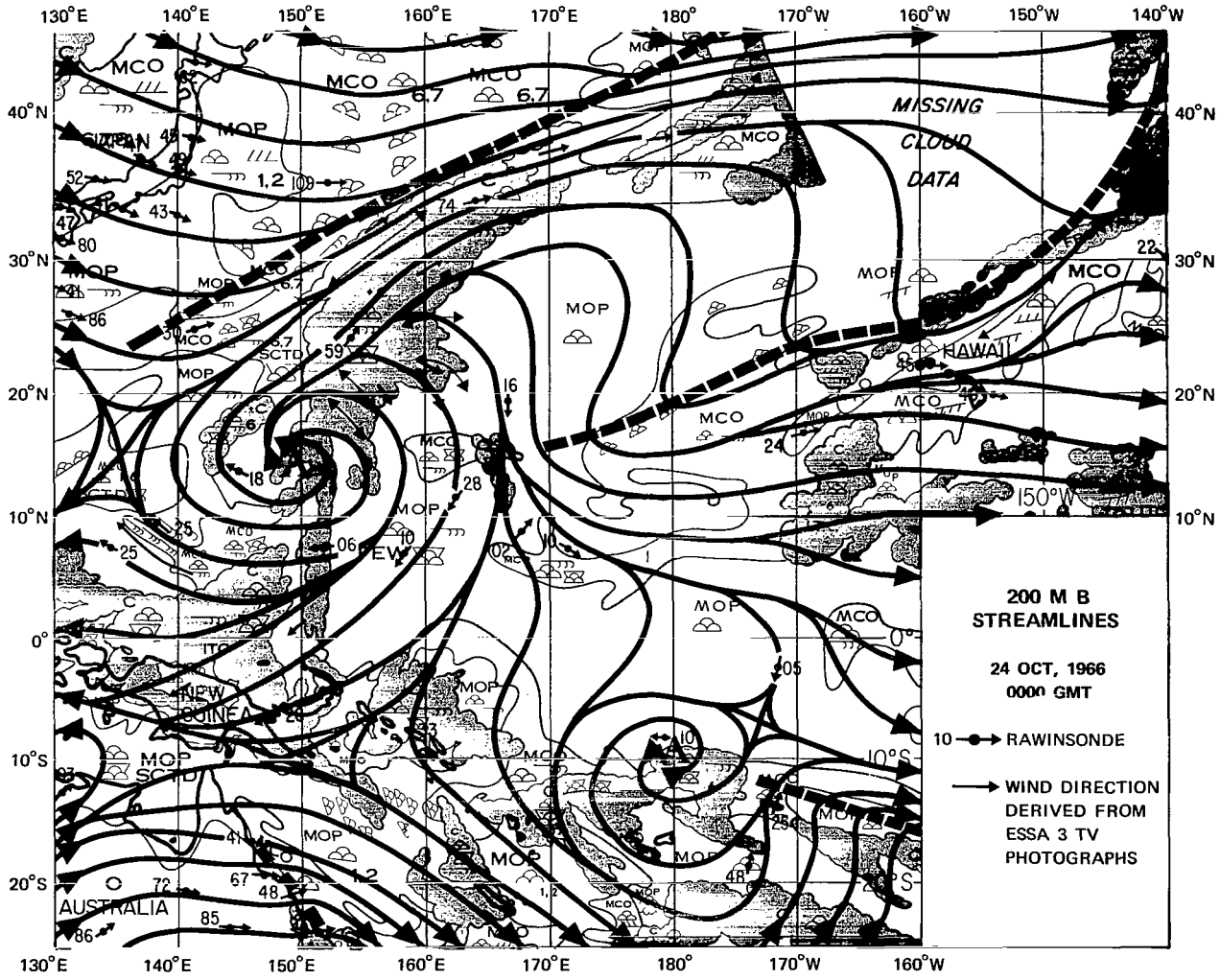


Figure A5—Composite of nephanalysis (based on satellite photographs, ESSA 1968) and 200-mb streamlines (derived from radiosonde observations and satellite photographs) on October 24, 1966, 00 GMT.

Appendix B

## October 25, 1966

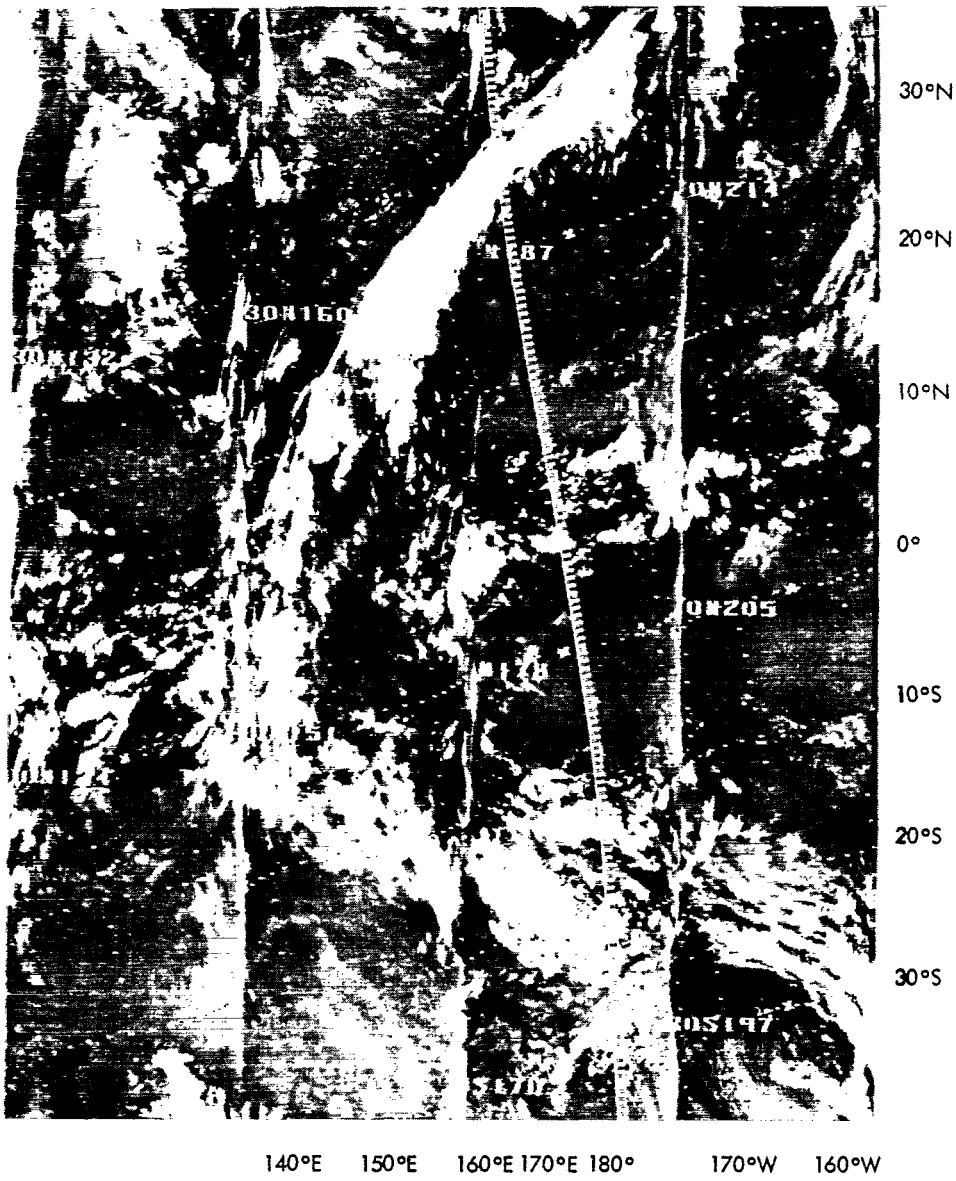


Figure B1—Montage of Nimbus II HRIR filmstrips (orbits 2171, 2172, 2173, and 2174) on October 25, 1966, near 1200 GMT (near local midnight). The dashed line is the 180° meridian.

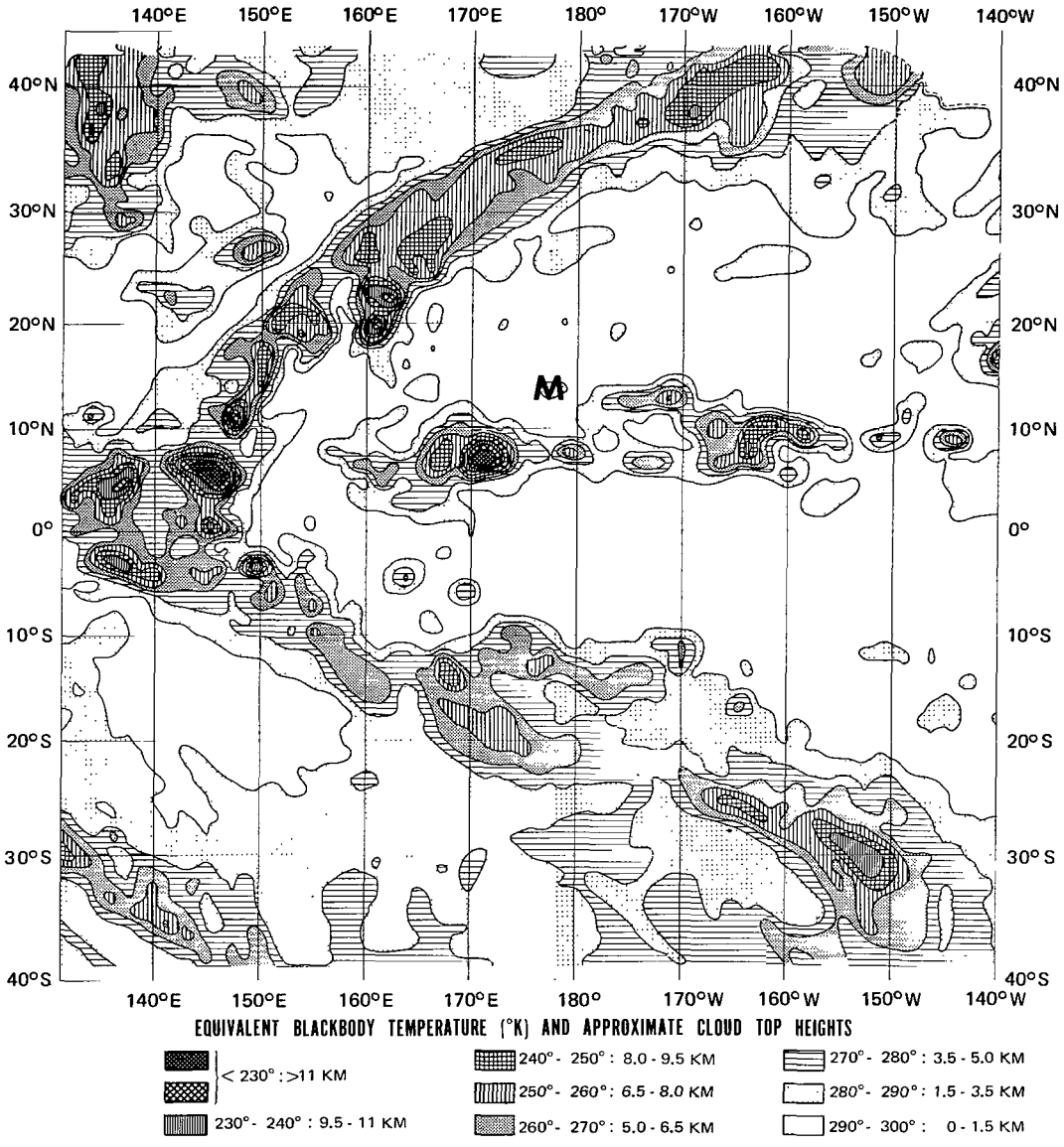


Figure B2—Analysis of Nimbus II HRIR measurements (orbits 2170, 2171, 2172, 2173, and 2174) on October 25, 1966, near 1200 GMT (near local midnight) based on a computer grid print map with 1.25 degrees longitude per grid interval.

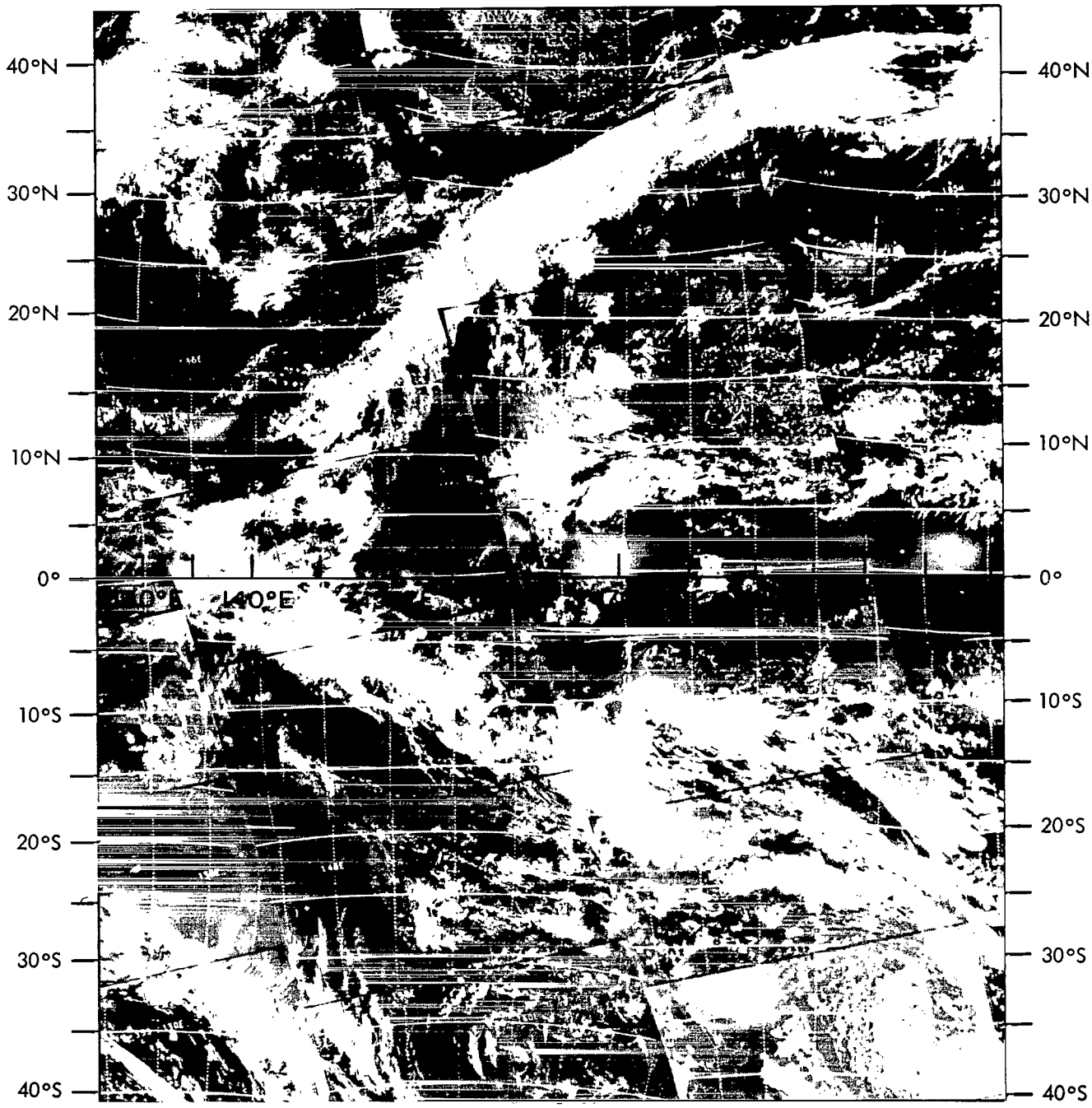


Figure B3—Montage of ESSA-3 television photographs (orbits 283, 284, 285, and 286) on October 25, 1966, near 0200 GMT (local early afternoon).

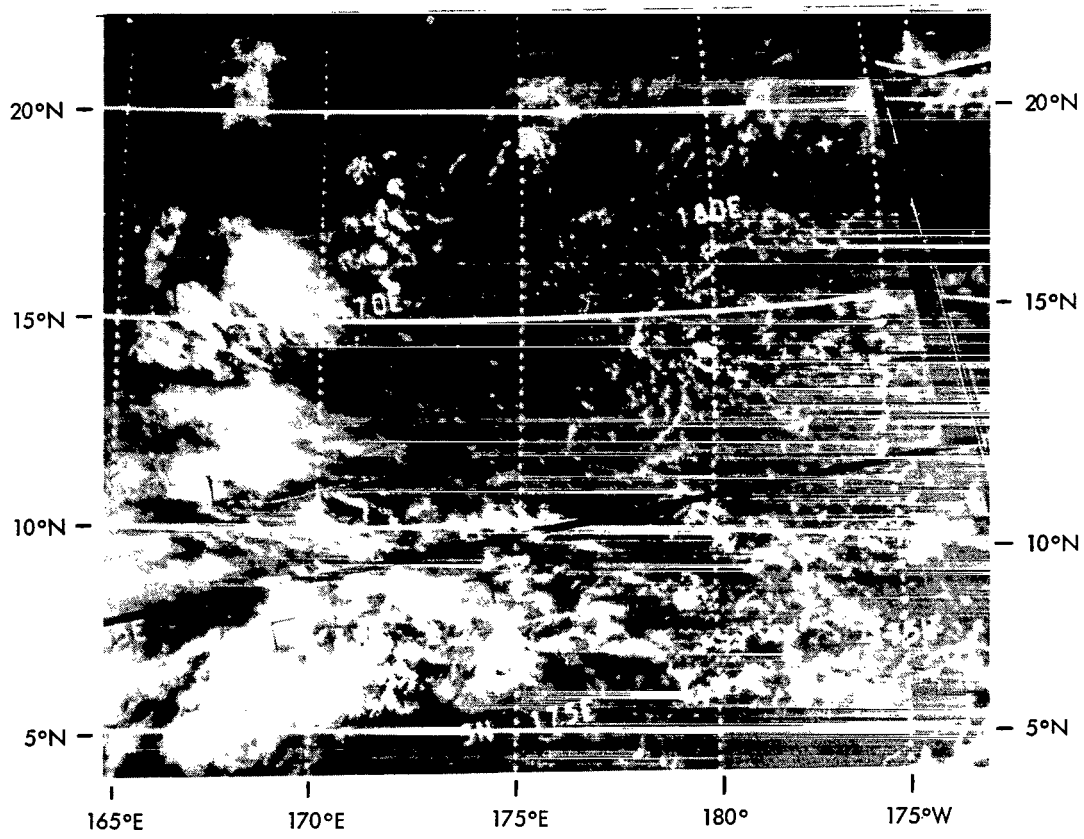


Figure B4—Montage of ESSA-3 television photographs (orbit 284) on October 25, 1966, near 0200 GMT (local early afternoon).

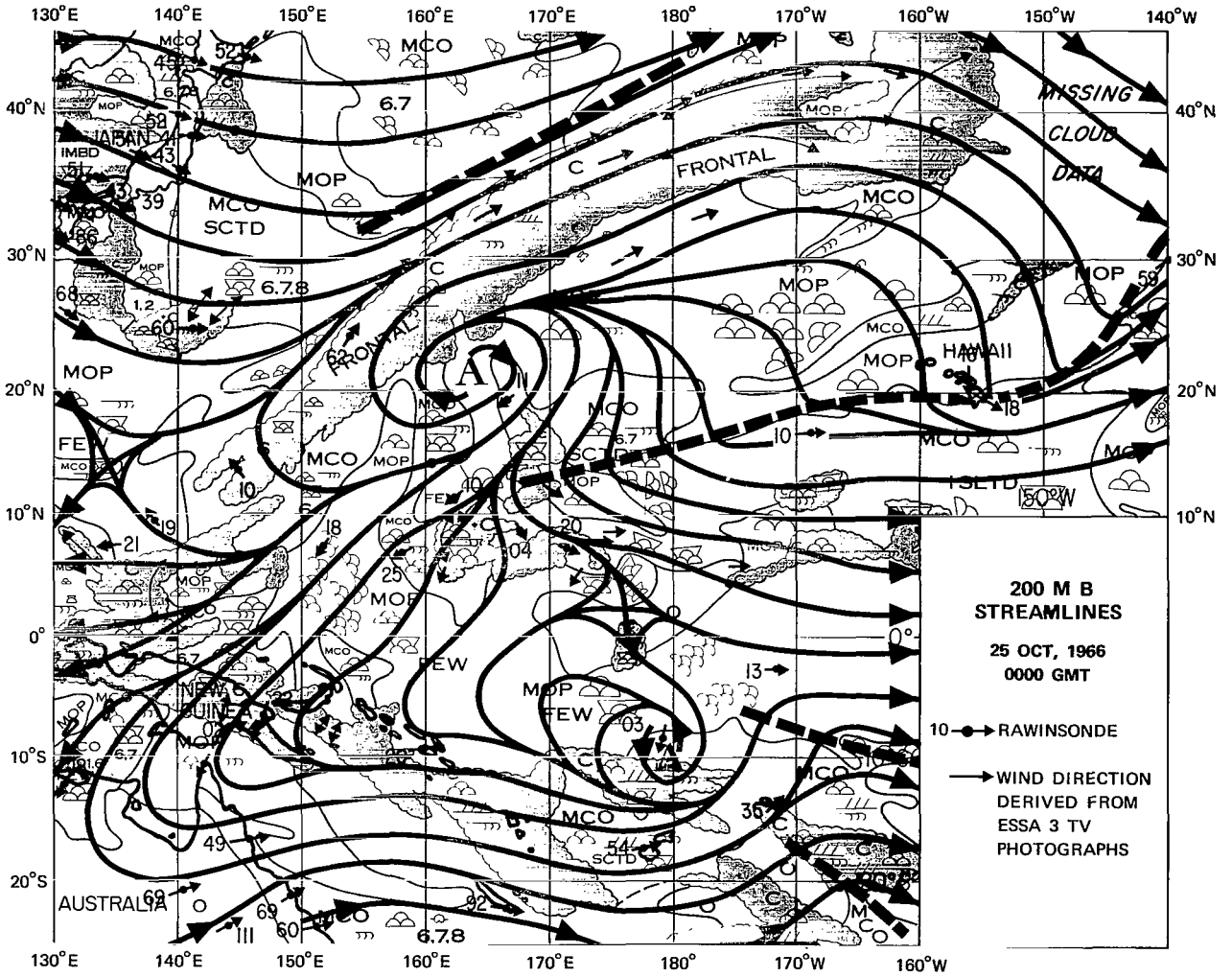


Figure B5—Composite of nephanalysis (based on satellite photographs, ESSA 1968) and 200-mb streamlines (derived from radiosonde observations and satellite photographs) on October 25, 1966, 00 GMT.

Appendix C

# October 26, 1966

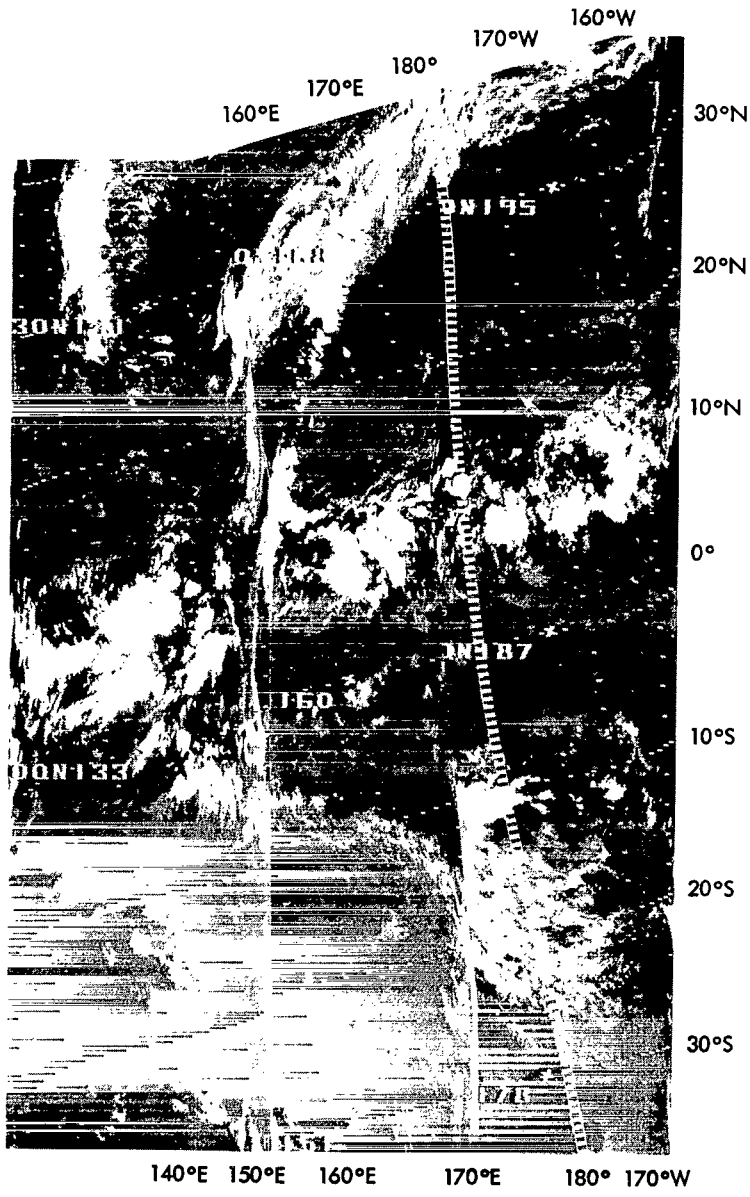


Figure C1—Montage of Nimbus II HRIR filmstrips (orbits 2185, 2186, and 2187) on October 26, 1966, near 1200 GMT (near local midnight). The dashed line is the 180° meridian.

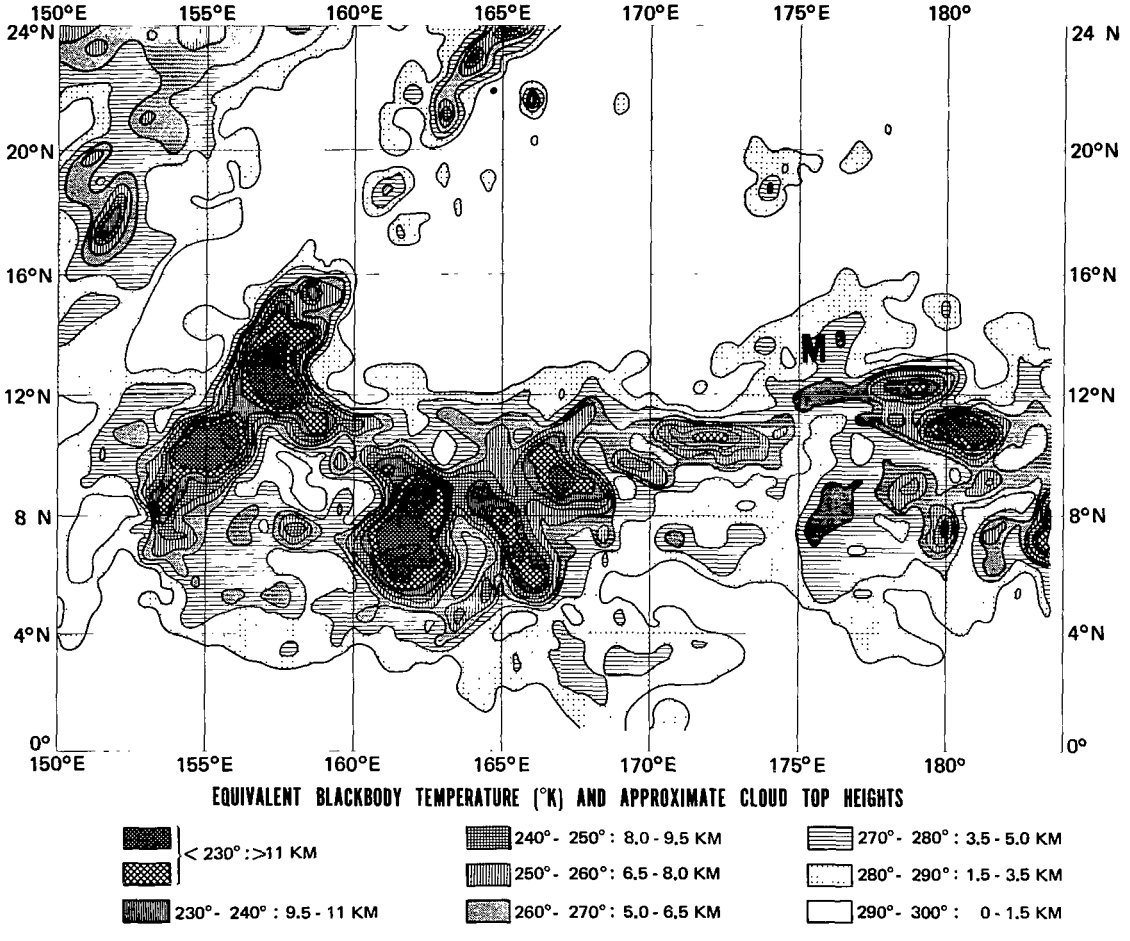


Figure C2—Analysis of Nimbus II HRIR measurements (orbits 2185, 2186, and 2187) on October 26, 1966, near 1200 GMT (near local midnight) based on a computer grid print map with 0.5 degree longitude per grid interval.

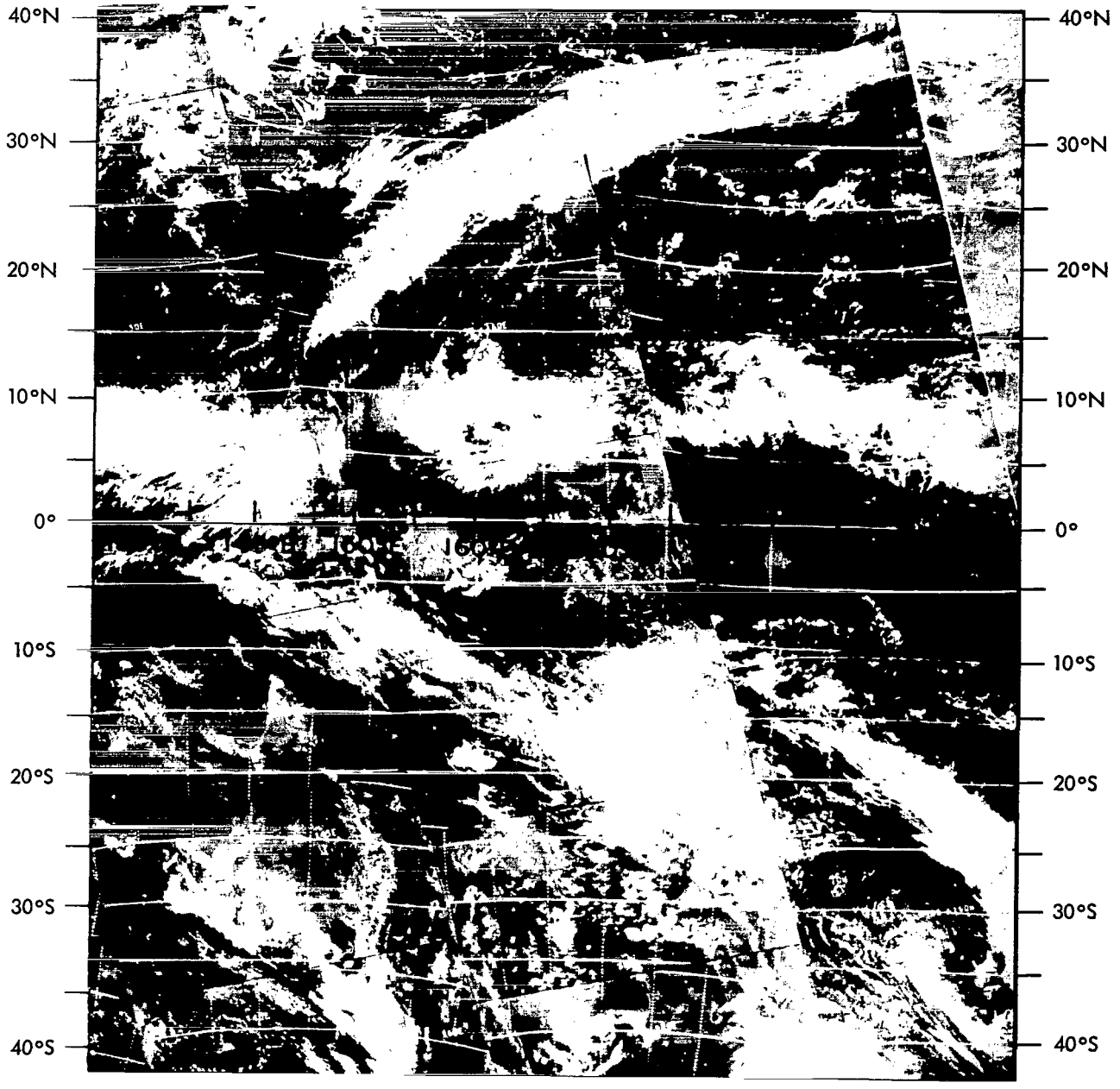


Figure C3—Montage of ESSA-3 television photographs (orbits 295, 296, 297, and 298) on October 26, 1966, near 0200 GMT (local early afternoon).

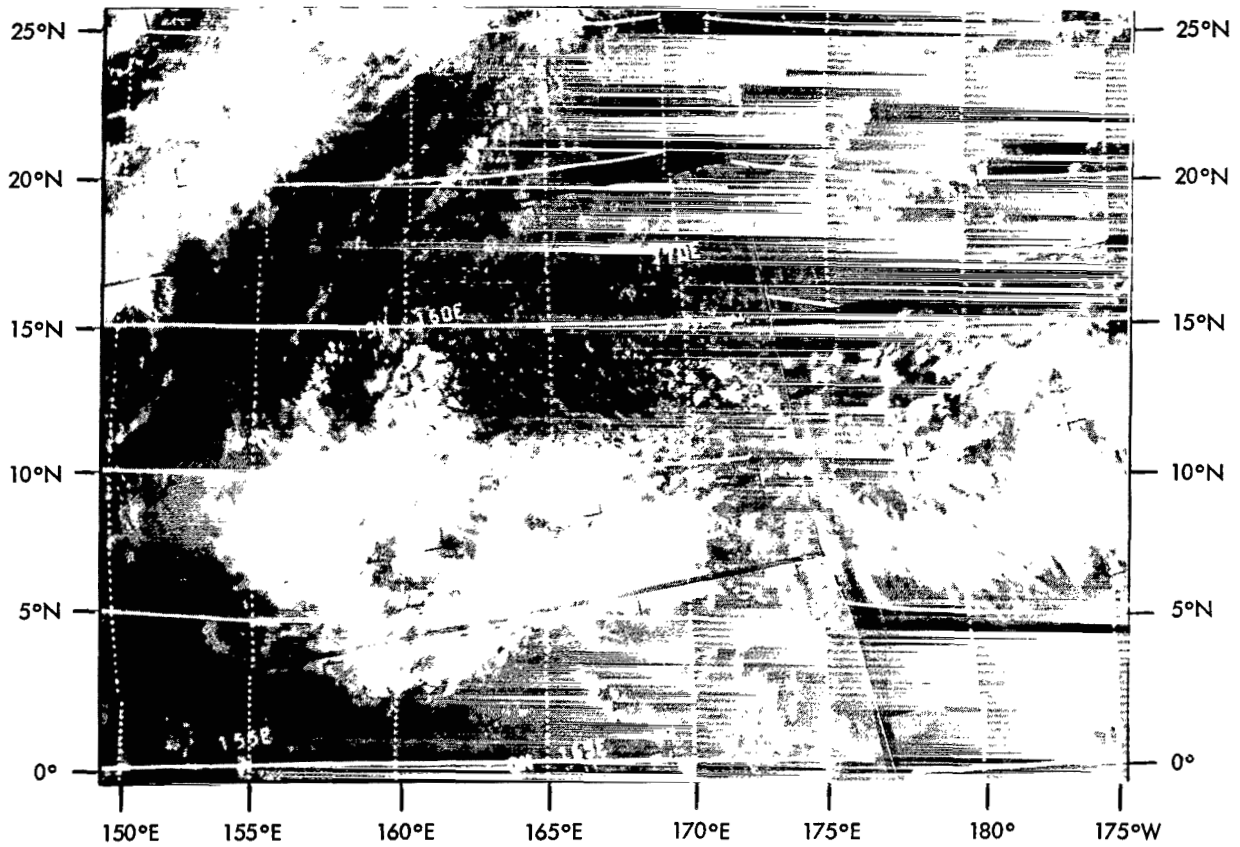


Figure C4—Montage of ESSA-3 television photographs (orbits 296 and 297) on October 26, 1966, near 0200 GMT (local early afternoon).

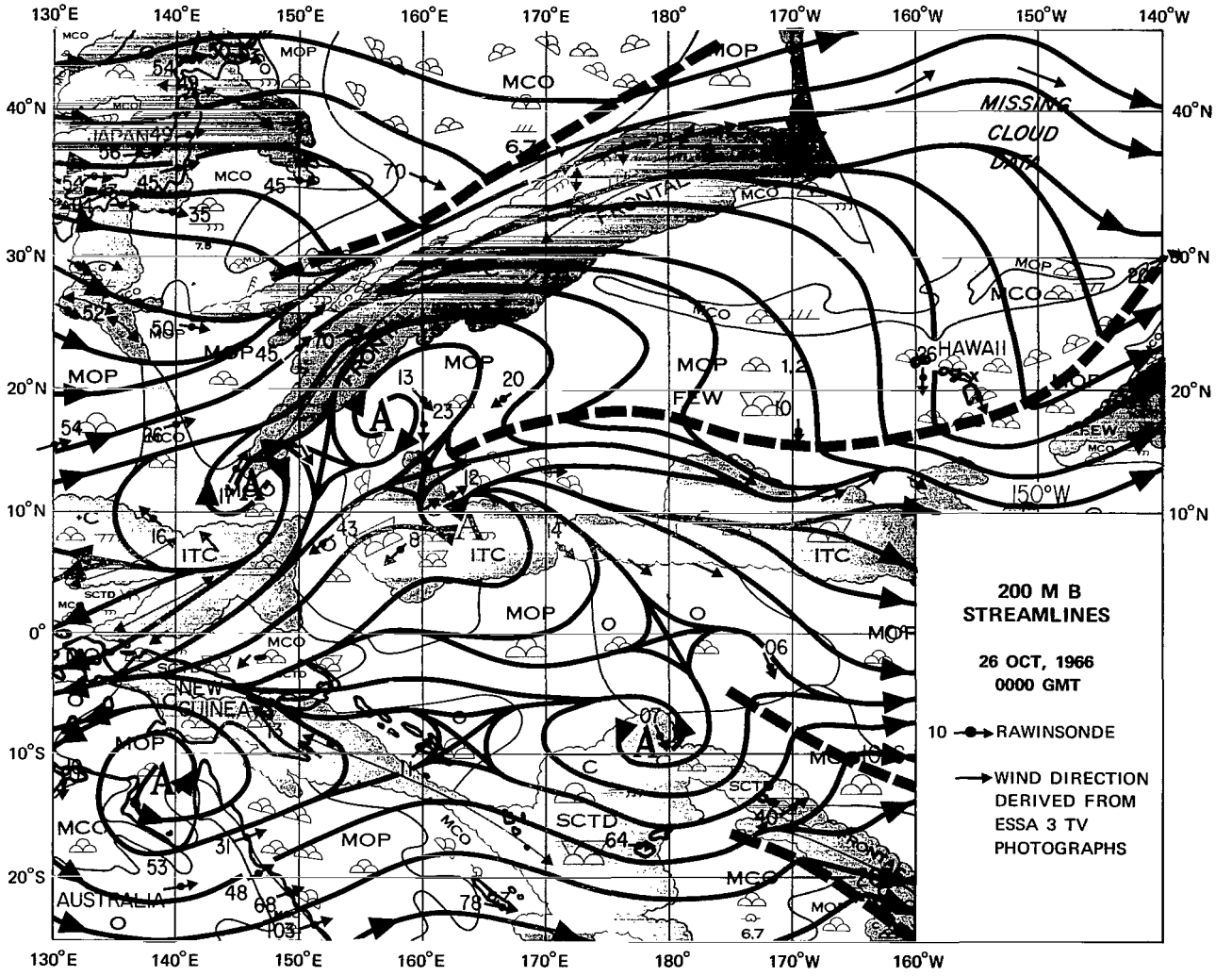


Figure C5—Composite of nephanalysis (based on satellite photographs, ESSA 1968) and 200-mb streamlines (derived from radiosonde observations and satellite photographs) on October 26, 1966, 00 GMT.

Appendix D

## October 27, 1966

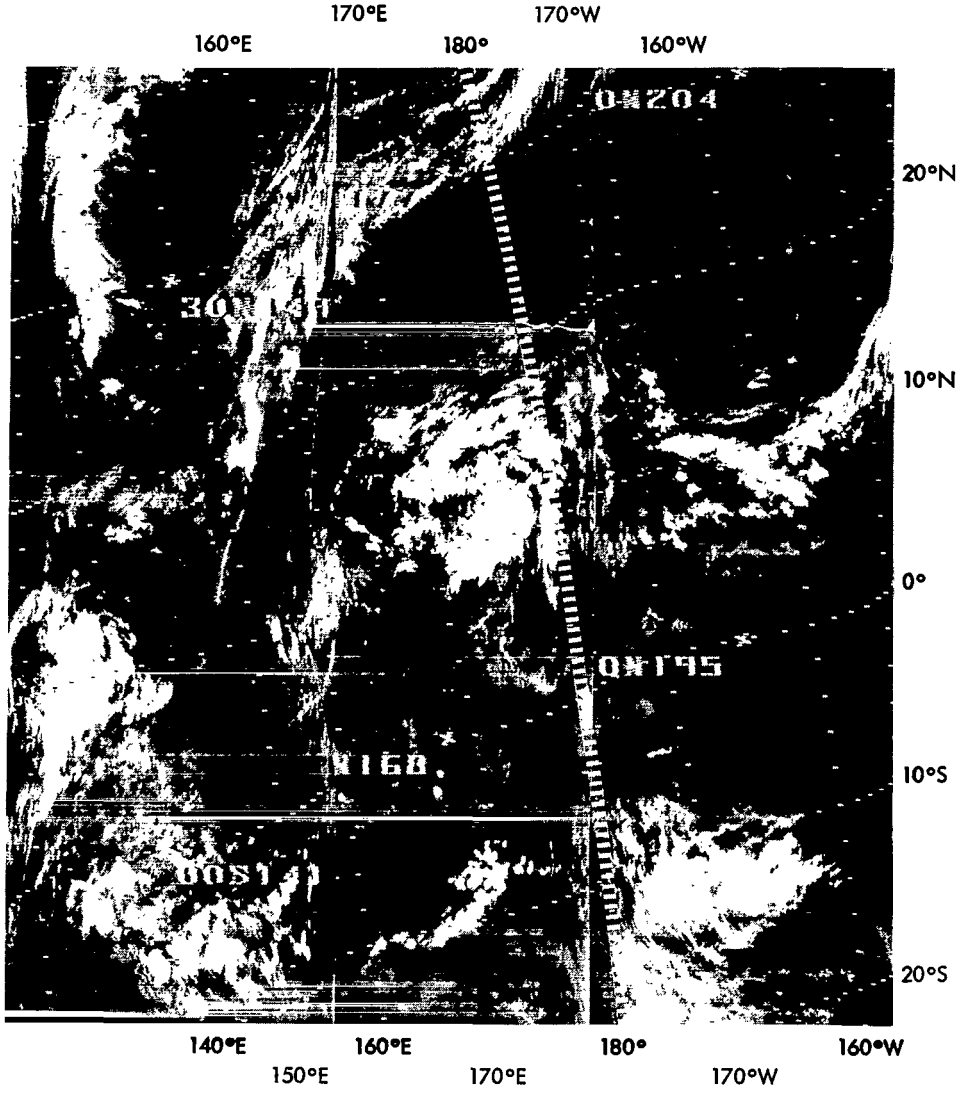


Figure D1—Montage of Nimbus II HRIR filmstrips (orbits 2198, 2199, and 2200) on October 27, 1966, near 1200 GMT (near local midnight). The dashed line is the 180° meridian.

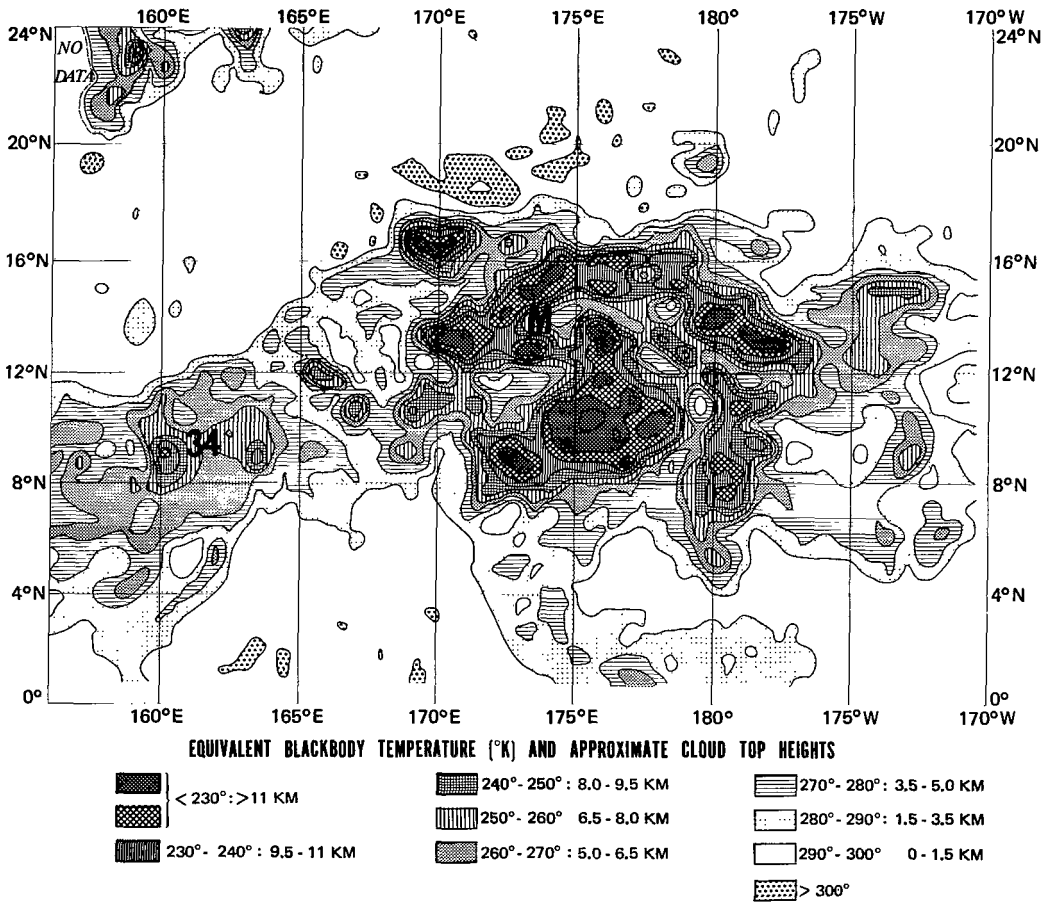


Figure D2—Analysis of Nimbus II HRIR measurements (orbits 2198, 2199, and 2200) on October 27, 1966, near 1200 GMT (near local midnight) based on a computer grid print map with 0.5 degrees longitude per grid interval.

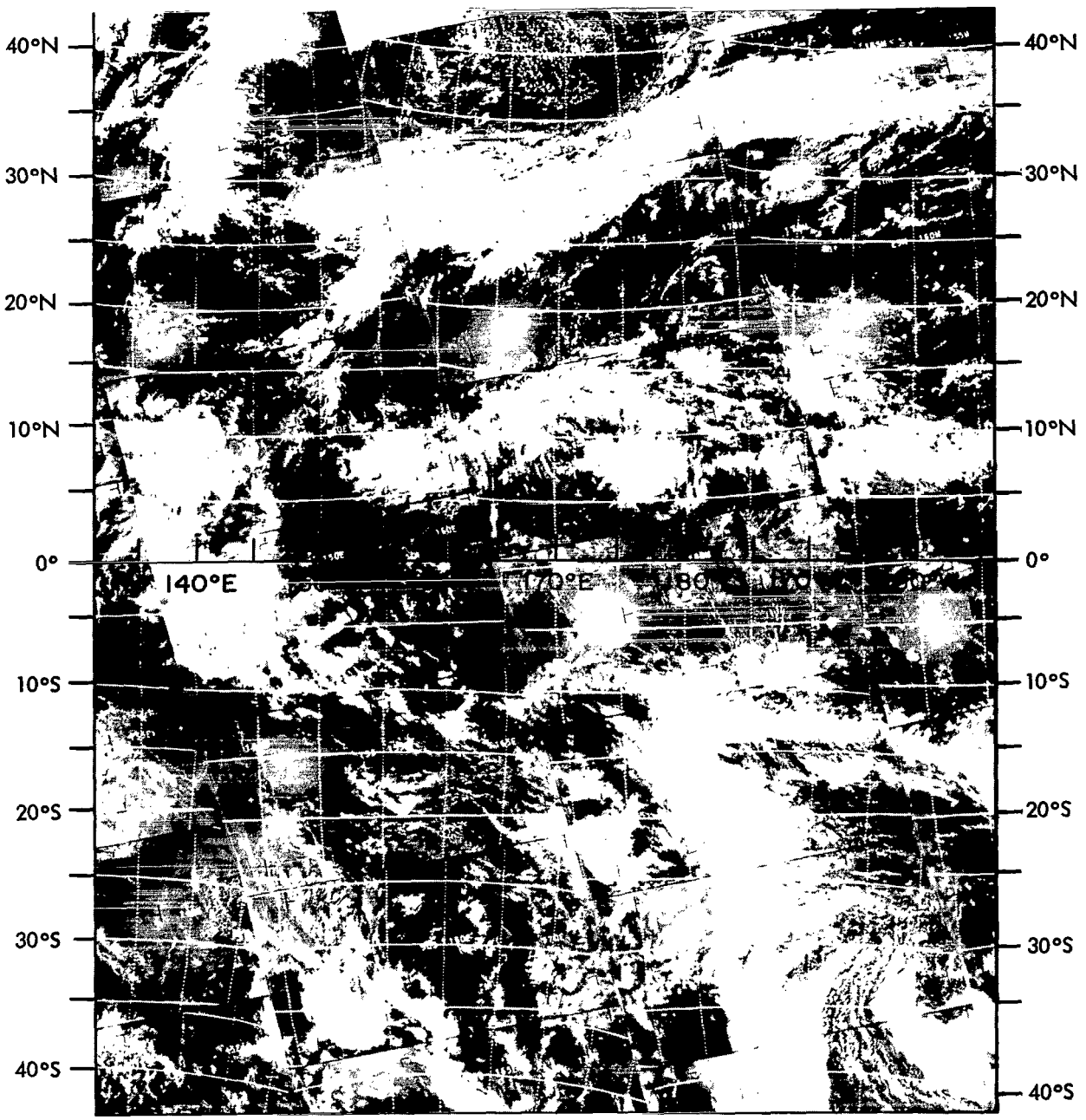


Figure D3—Montage of ESSA-3 television photographs (orbits 308, 309, 310, and 311) on October 27, 1966, near 0200 GMT (local early afternoon).

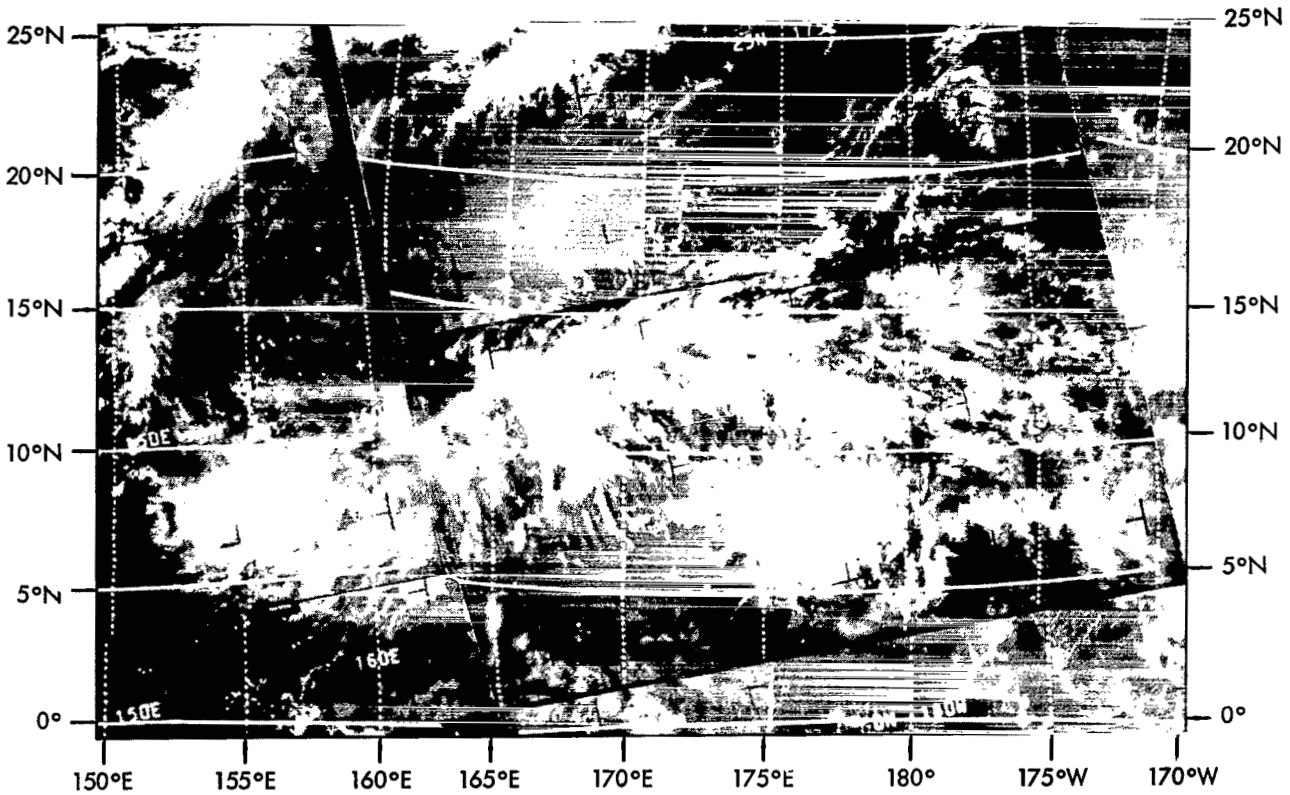


Figure D4—Montage of ESSA-3 television photographs (orbits 309 and 310) on October 27, 1966, near 0200 GMT (local early afternoon).

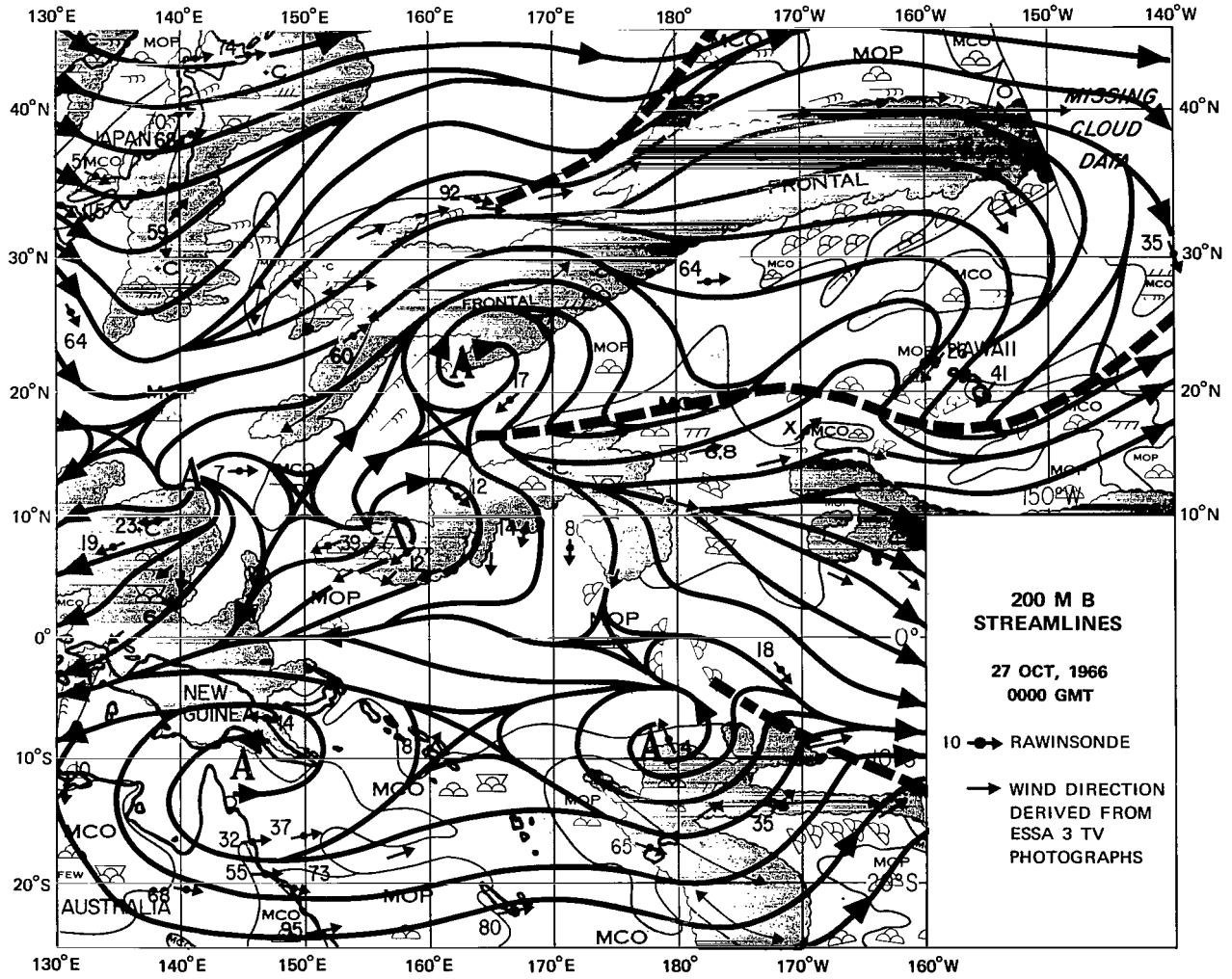


Figure D5—Composite of nephanalysis (based on satellite photographs, ESSA 1968) and 200-mb streamlines (derived from radiosonde observations and satellite photographs) on October 27, 1966, 00 GMT.

Appendix E

## October 28, 1966

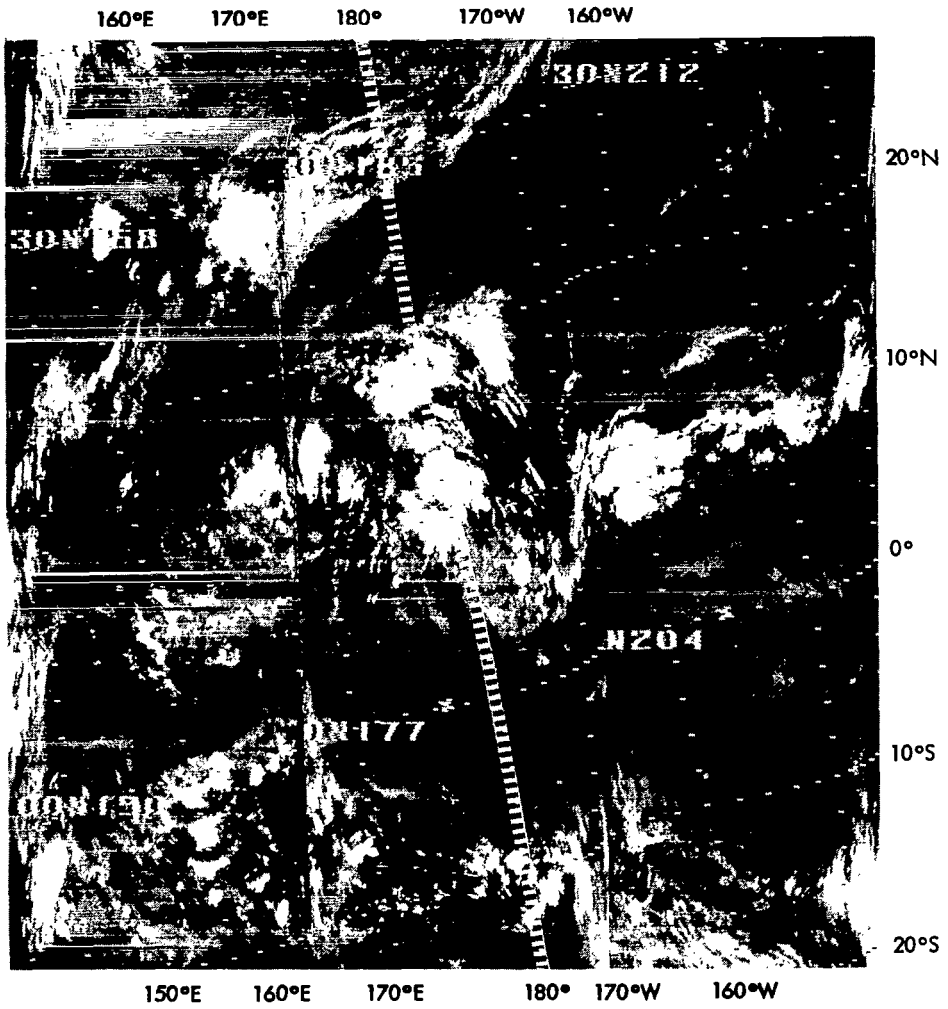


Figure E1—Montage of Nimbus II HRIR filmstrips (orbits 2211, 2212, and 2213) on October 28, 1966, near 1200 GMT (near local midnight). The dashed line is the 180° meridian.

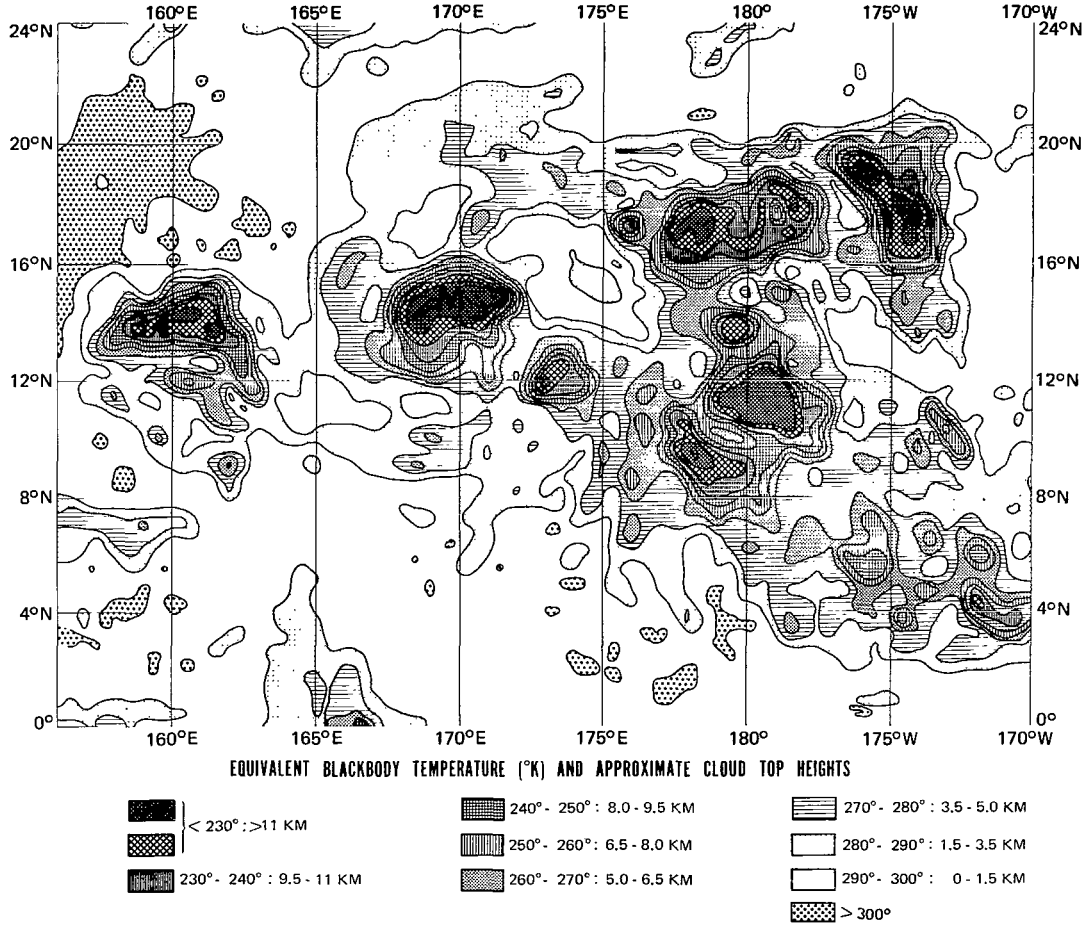


Figure E2—Analysis of Nimbus II HRIR measurements (orbits 2212 and 2213) on October 28, 1966, near 1200 GMT (near local midnight) based on a computer grid map with 0.5 degree longitude per grid interval.

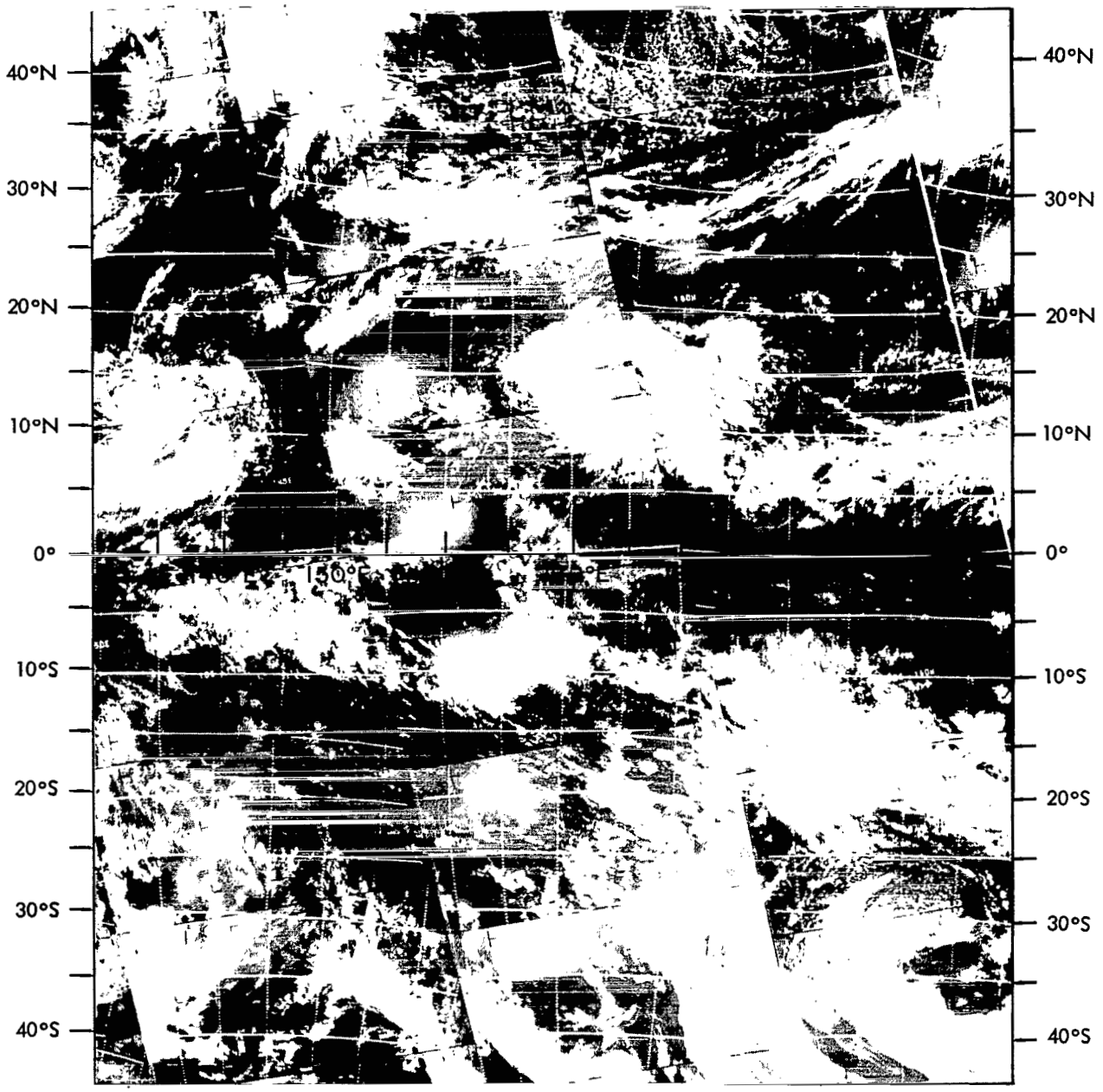


Figure E3—Montage of ESSA-3 television photographs (orbits 320, 321, 322, and 323) on October 28, 1966, near 0200 GMT (local early afternoon).

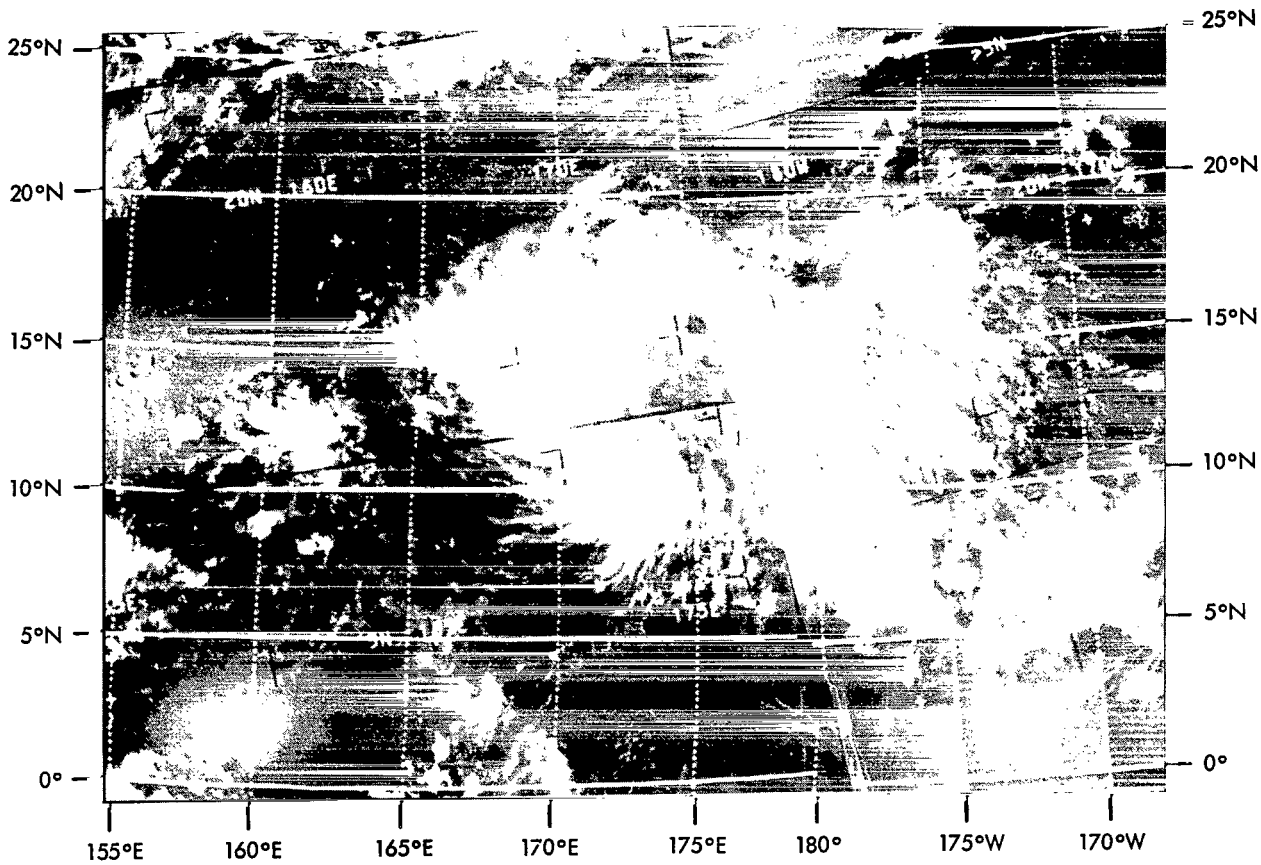


Figure E4—Montage of ESSA-3 television photographs (orbits 321 and 322) on October 28, 1966, near 0200 GMT (local early afternoon).

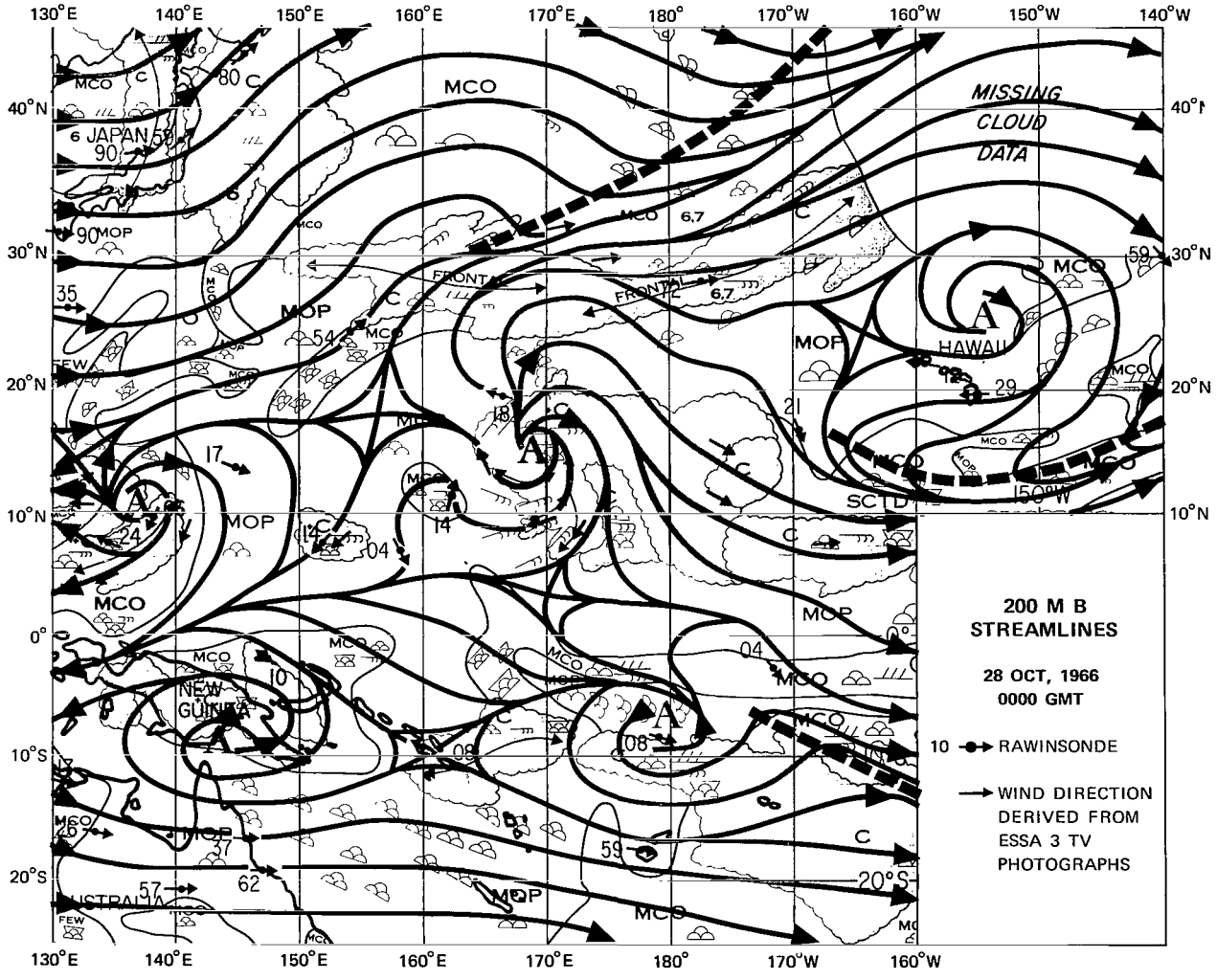


Figure E5—Composite of nephanalysis (based on satellite photographs, ESSA 1968) and 200-mb streamlines (derived from radiosonde observations and satellite photographs) on October 28, 1966, 00 GMT.

Appendix F

## October 29, 1966

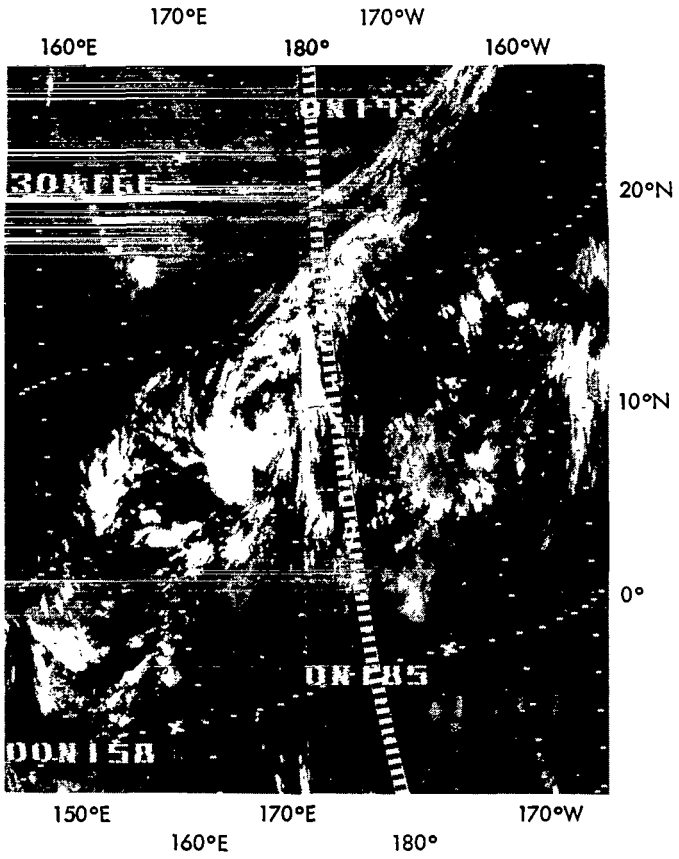


Figure F1—Montage of Nimbus II HRIR filmstrips (orbits 2225, and 2226) on October 29, 1966, near 1200 GMT (near local midnight). The dashed line is the 180° meridian.

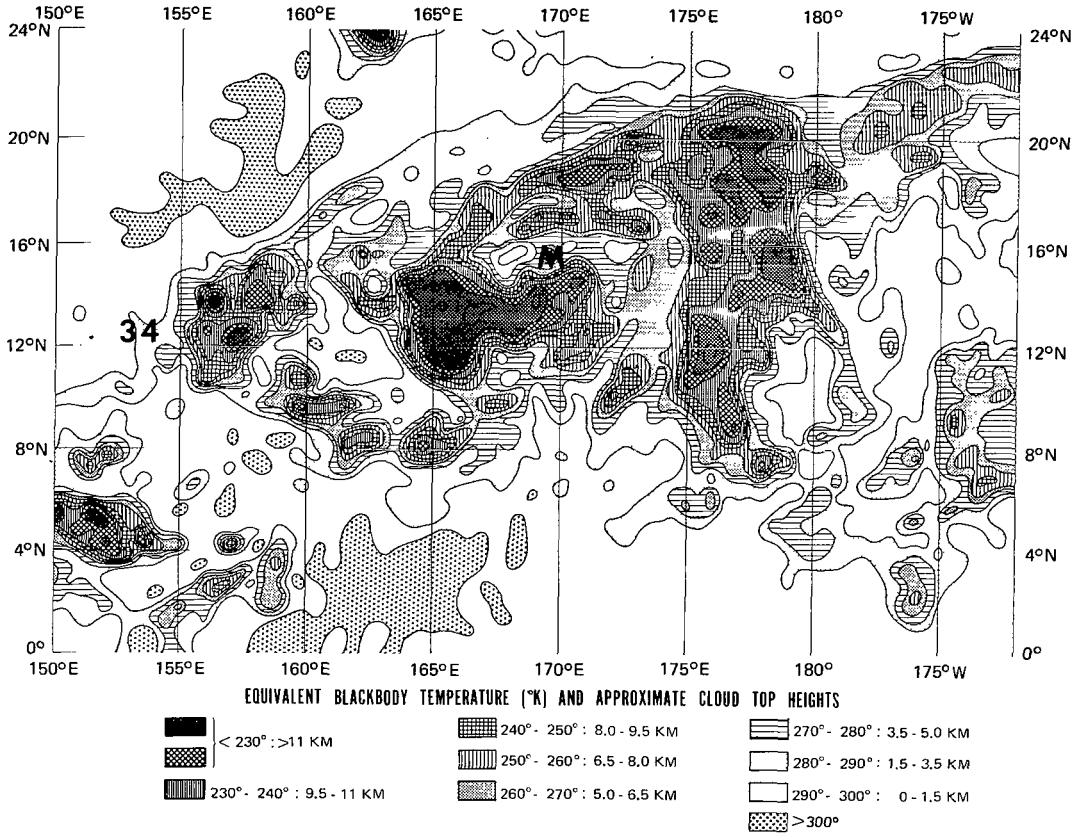


Figure F2—Analysis of Nimbus II HRIR measurements (orbits 2225, and 2226) on October 29, 1966, near 1200 GMT (near local midnight) based on a computer grid print map with 0.5 degree longitude per grid interval.

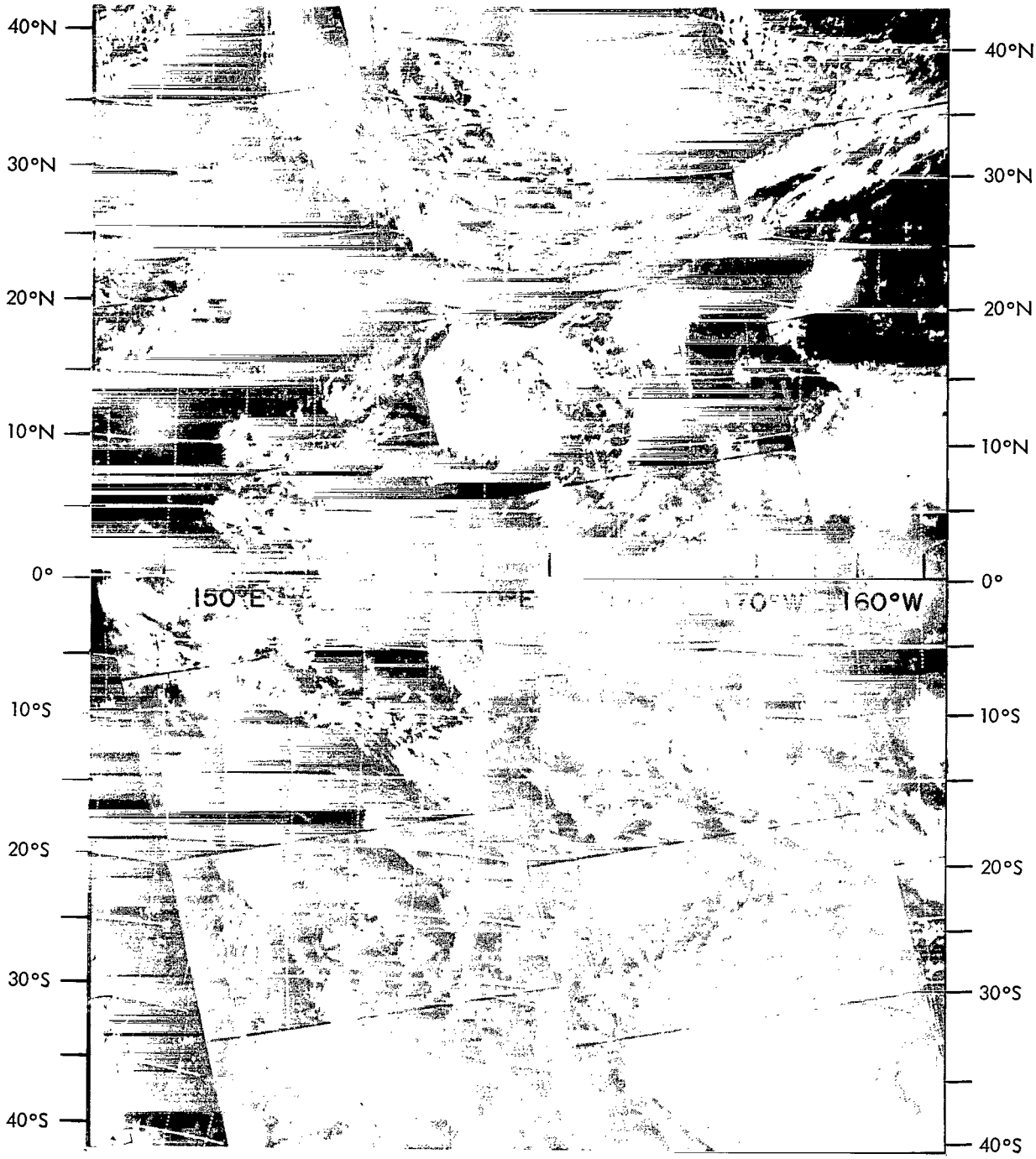


Figure F3—Montage of ESSA-3 television photographs (orbits 333, 334, 335, and 336) on October 29, 1966, near 0200 GMT (local early afternoon).

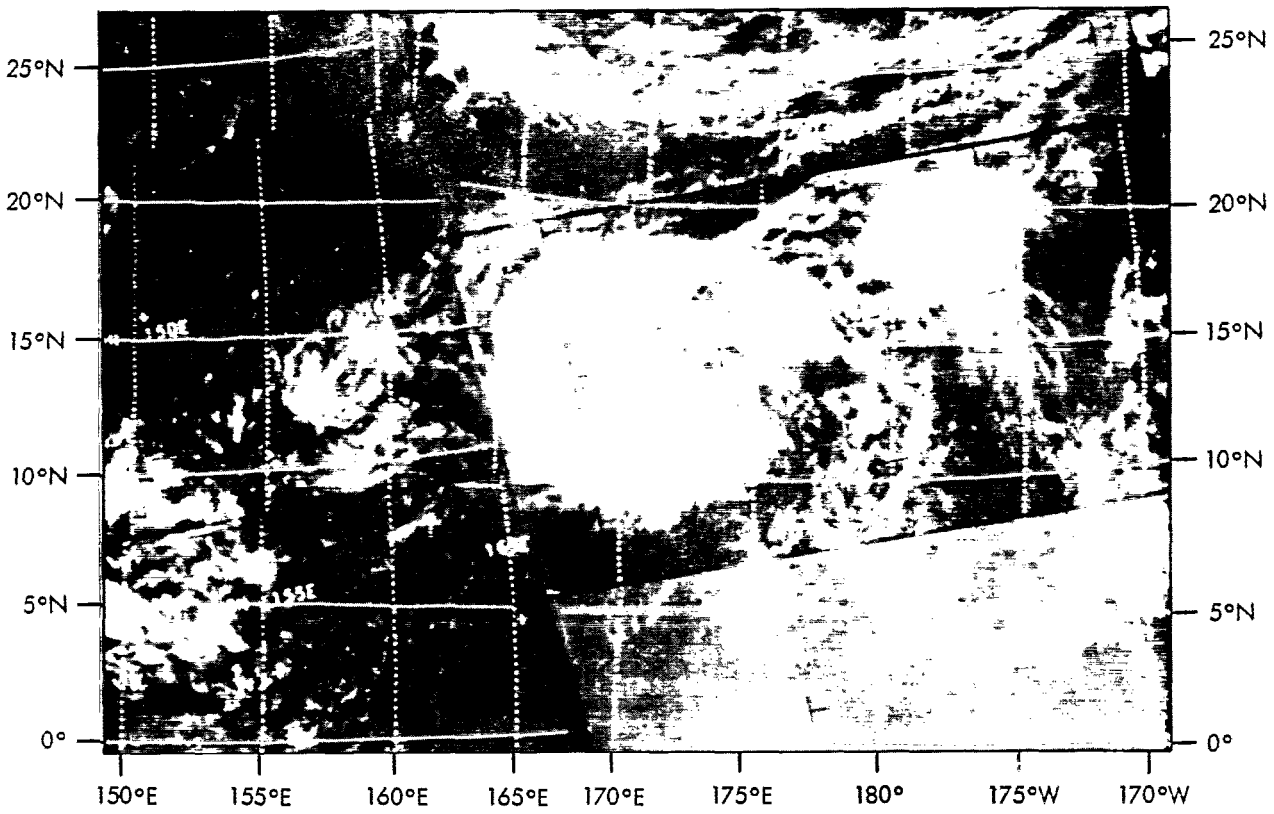


Figure F4—Montage of ESSA-3 television photographs (orbits 334, and 335) on October 29, 1966, near 0200 GMT (local early afternoon).

Appendix G

# October 30, 1966

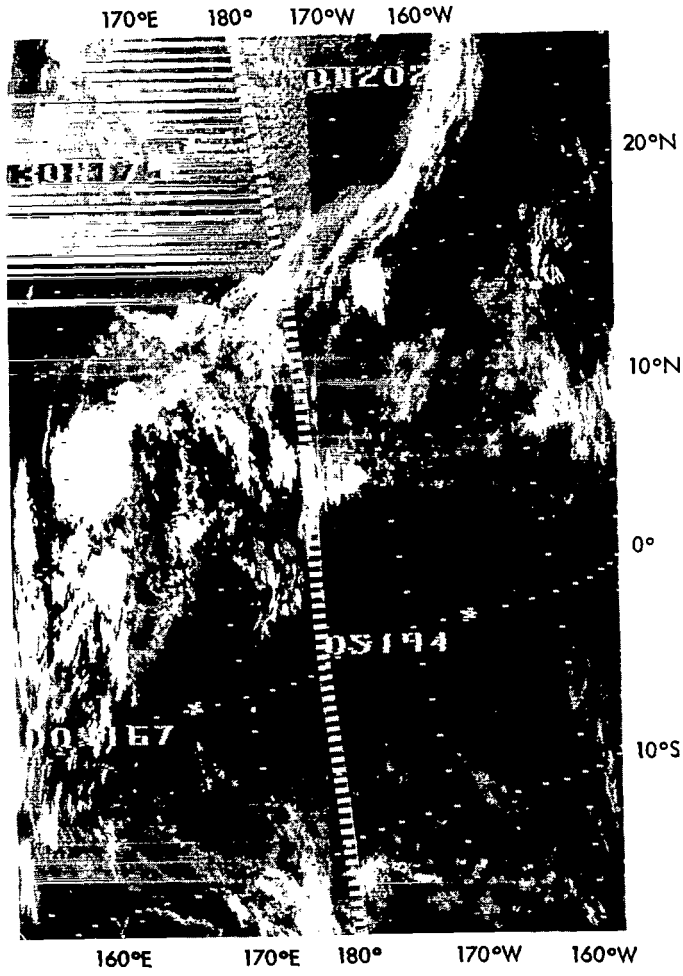


Figure G1—Montage of Nimbus II HRIR filmstrips (orbits 2238, and 2239) on October 30, 1966, near 1200 GMT (near local midnight). The dashed line is the 180° meridian.

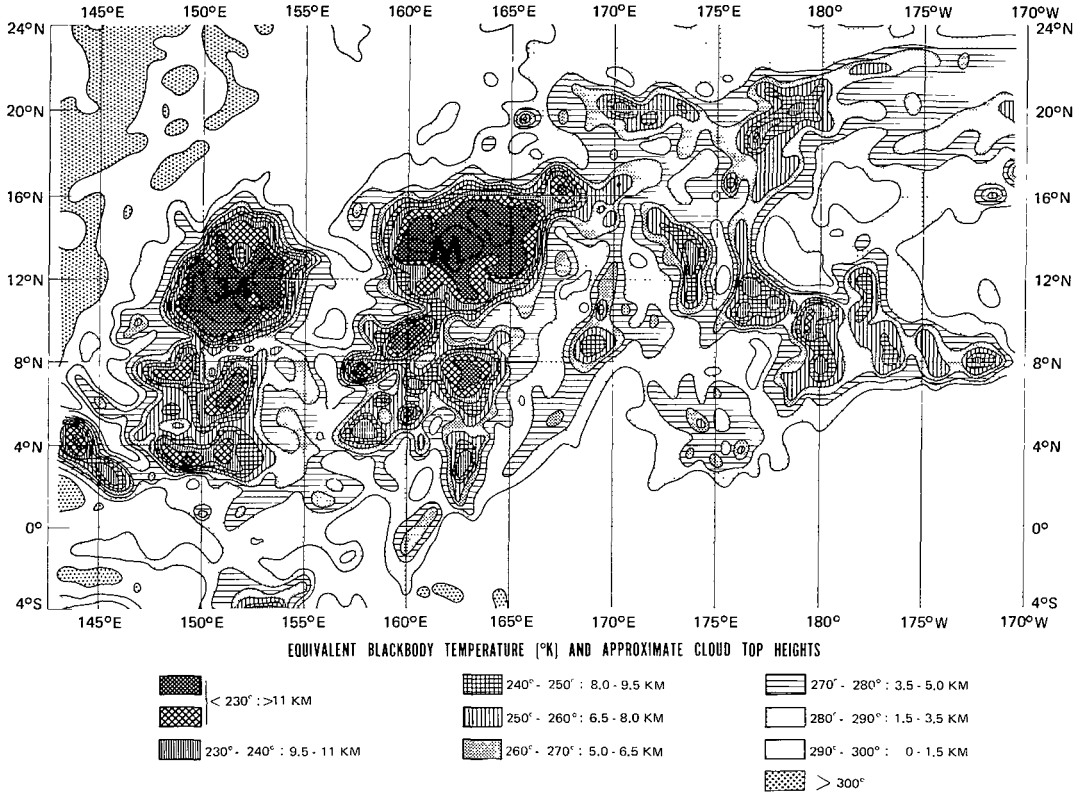


Figure G2—Analysis of Nimbus II HRIR measurements (orbits 2238, 2239, and 2240) on October 30, 1966, near 1200 GMT (near local midnight) based on a computer grid print map with 0.625 degree longitude per grid interval.

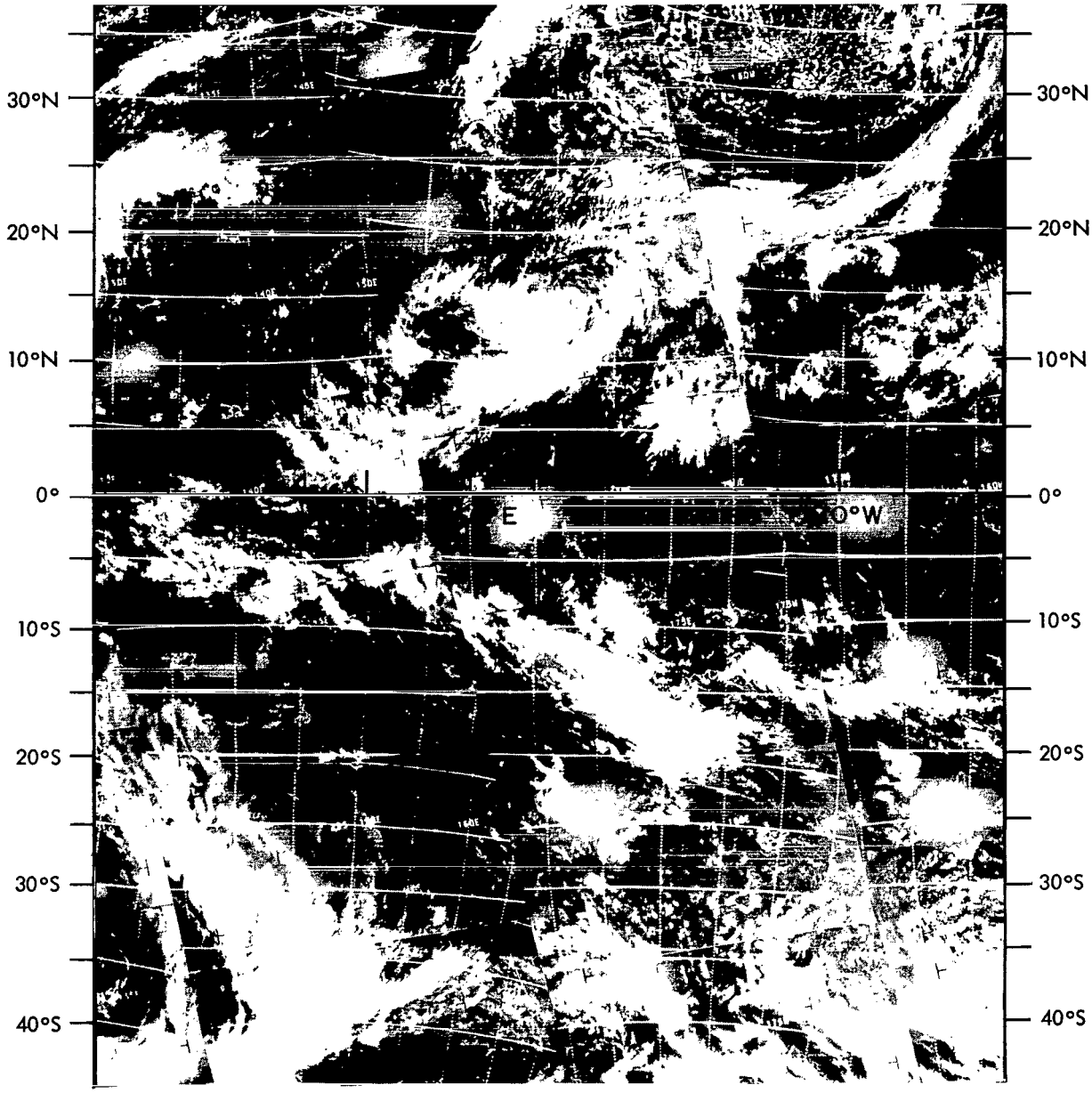


Figure G3—Montage of ESSA-3 television photographs (orbits 346, 347, and 348) on October 30, 1966, near 0200 GMT (local early afternoon).

Appendix H

## October 31, 1966

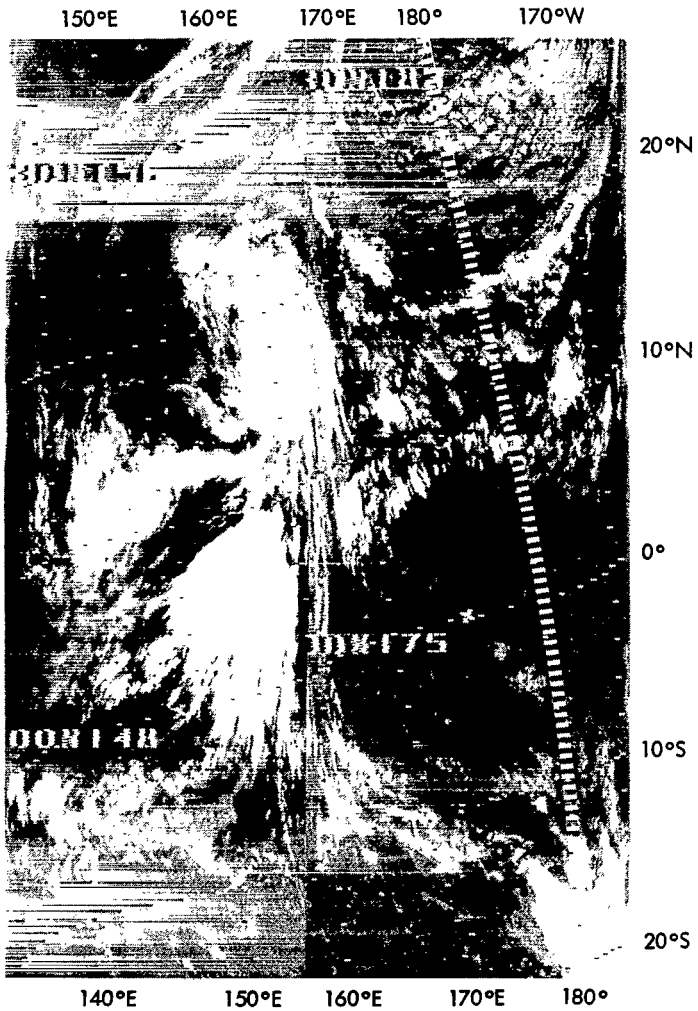


Figure H1—Montage of Nimbus II HRIR filmstrips (orbits 2252, and 2253) on October 31, 1966, near 1200 GMT (near local midnight). The dashed line is the 180° meridian.

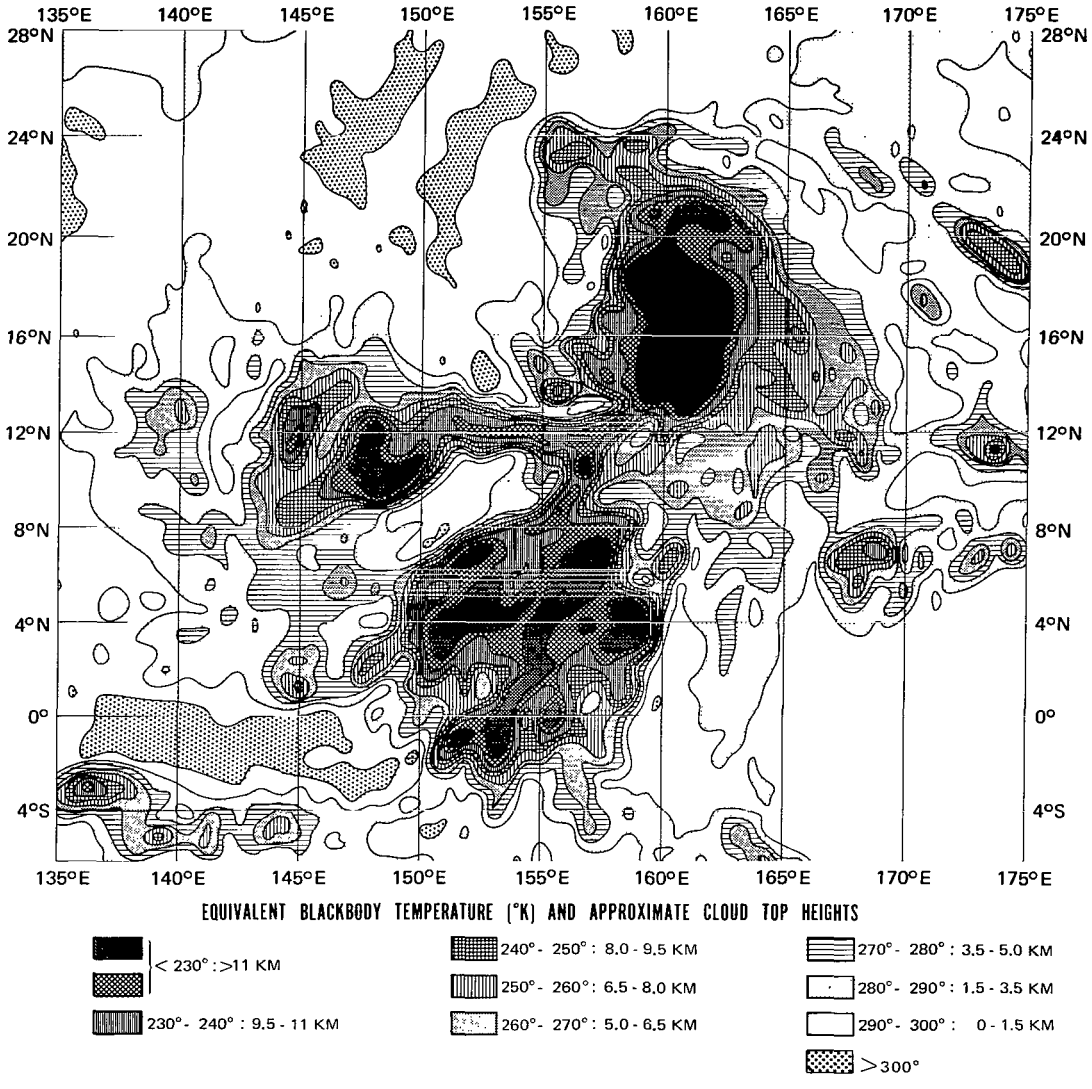


Figure H2—Analysis of Nimbus II HRIR measurements (orbits 2252, 2253, and 2254) on October 31, 1966, near 1200 GMT (near local midnight) based on a computer grid print map with 0.625 degree longitude per grid interval.

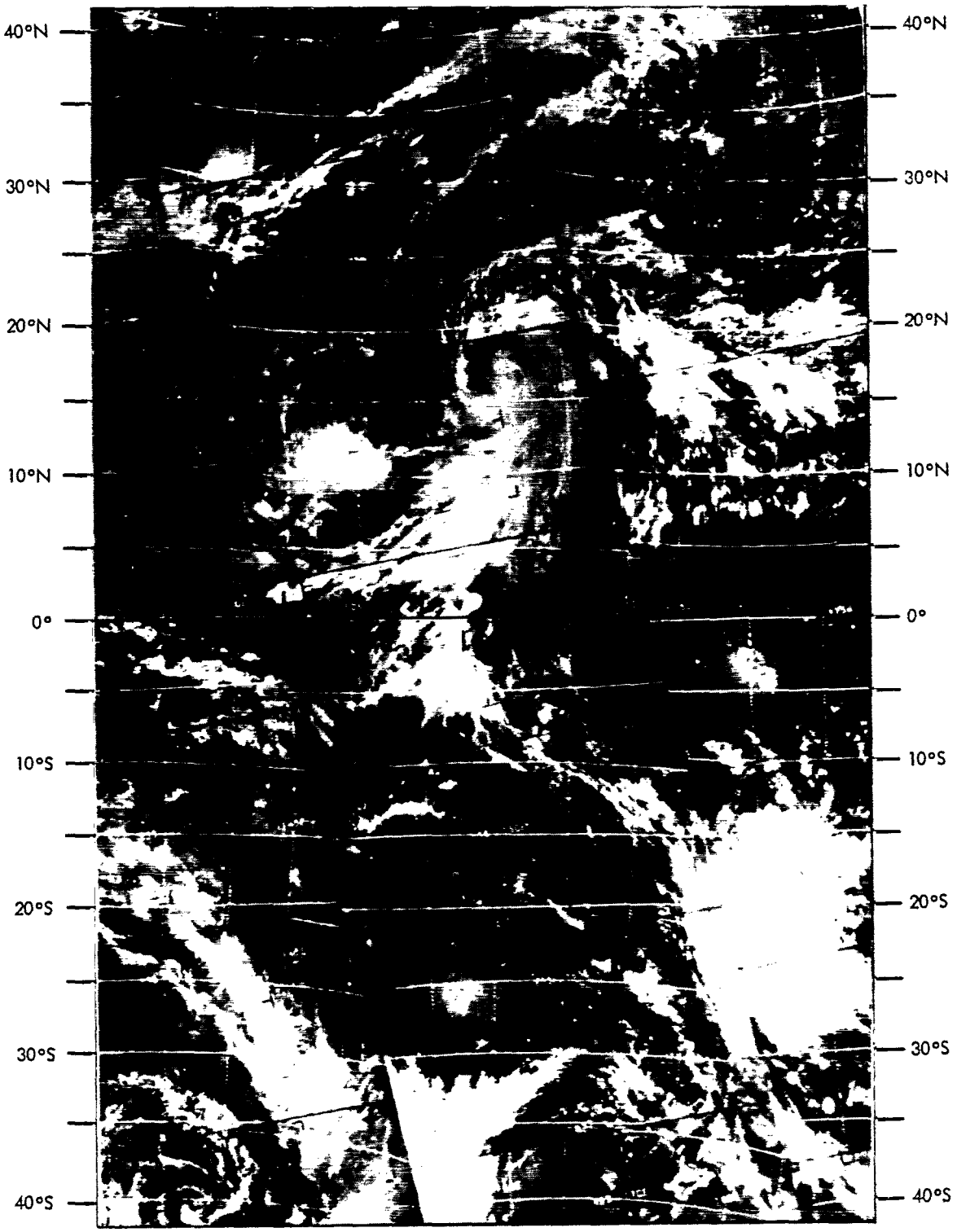


Figure H3—Montage of ESSA-3 television photographs (orbits 360, 361, and 362) on October 31, 1966, near 0200 GMT (local early afternoon).

Appendix I

# November 1, 1966

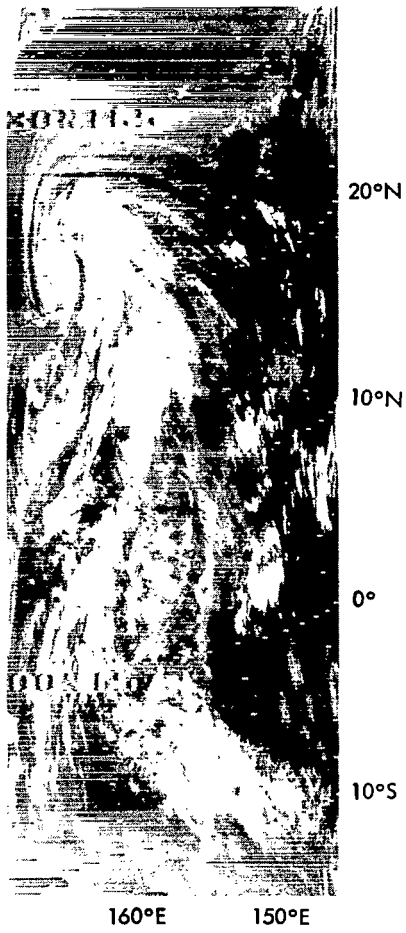


Figure 11—Nimbus II HRIR filmstrip (orbit 2266) on November 1, 1966, near 1200 GMT (near local midnight).

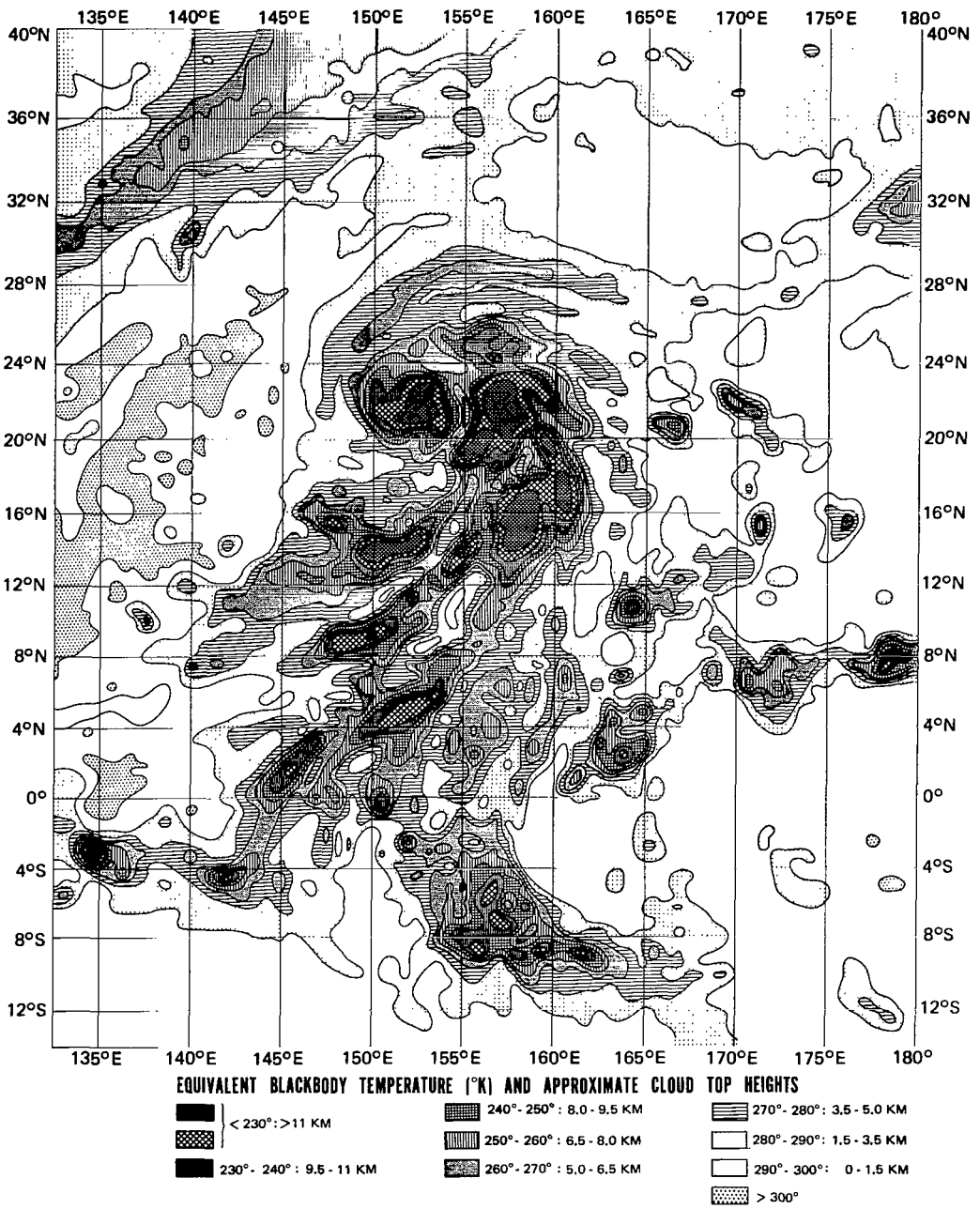


Figure 12—Analysis of Nimbus II HRIR measurements (orbits 2265, 2266, and 2267) on November 1, 1966, near 1200 GMT (near local midnight) based on a computer grid print map with 0.625 degree longitude per grid interval.

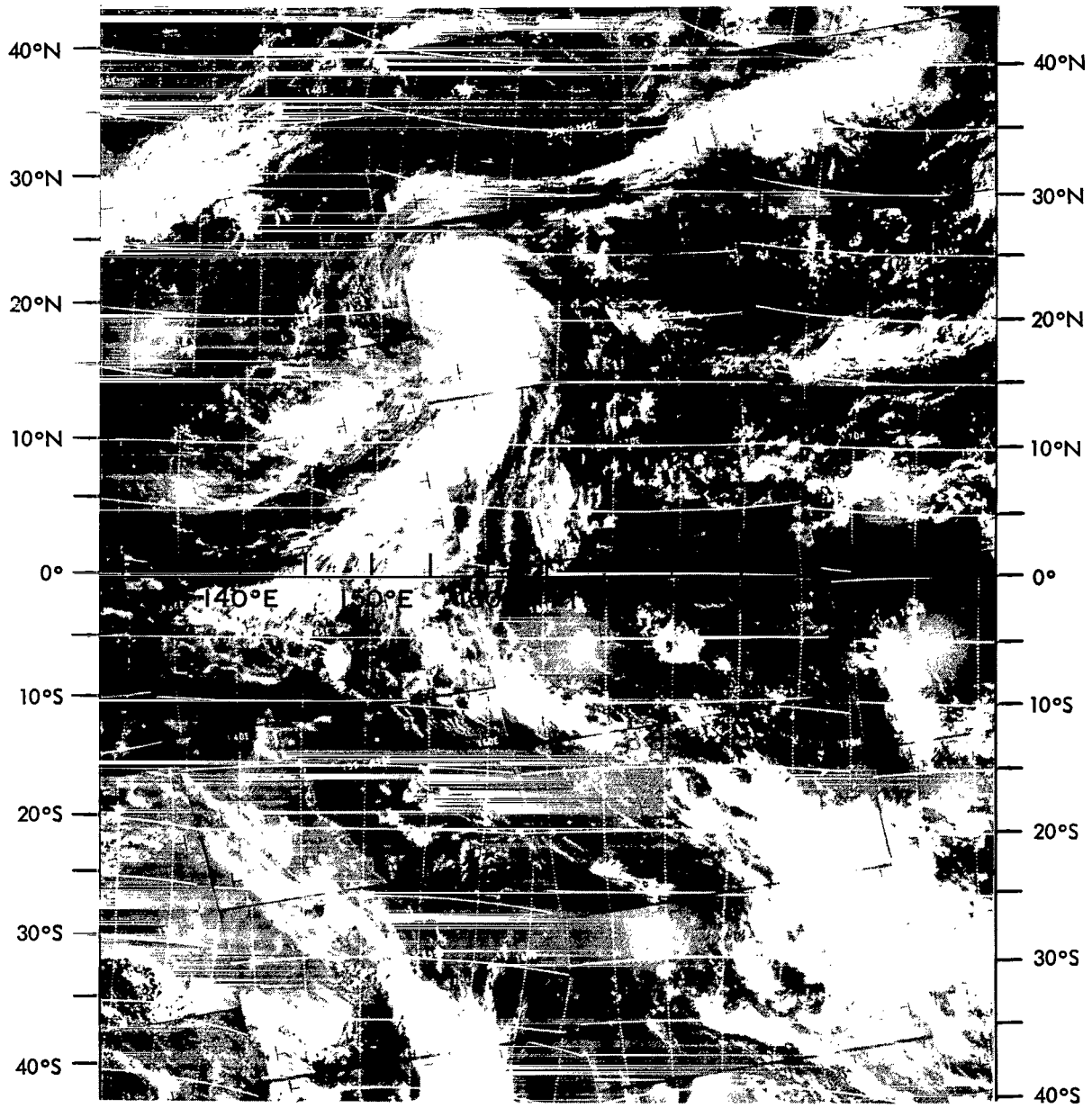


Figure 13—Montage of ESSA-3 television photographs (orbits 371, 372, and 373) on November 1, 1966 (local early afternoon).

Appendix J

**November 2, 1966**

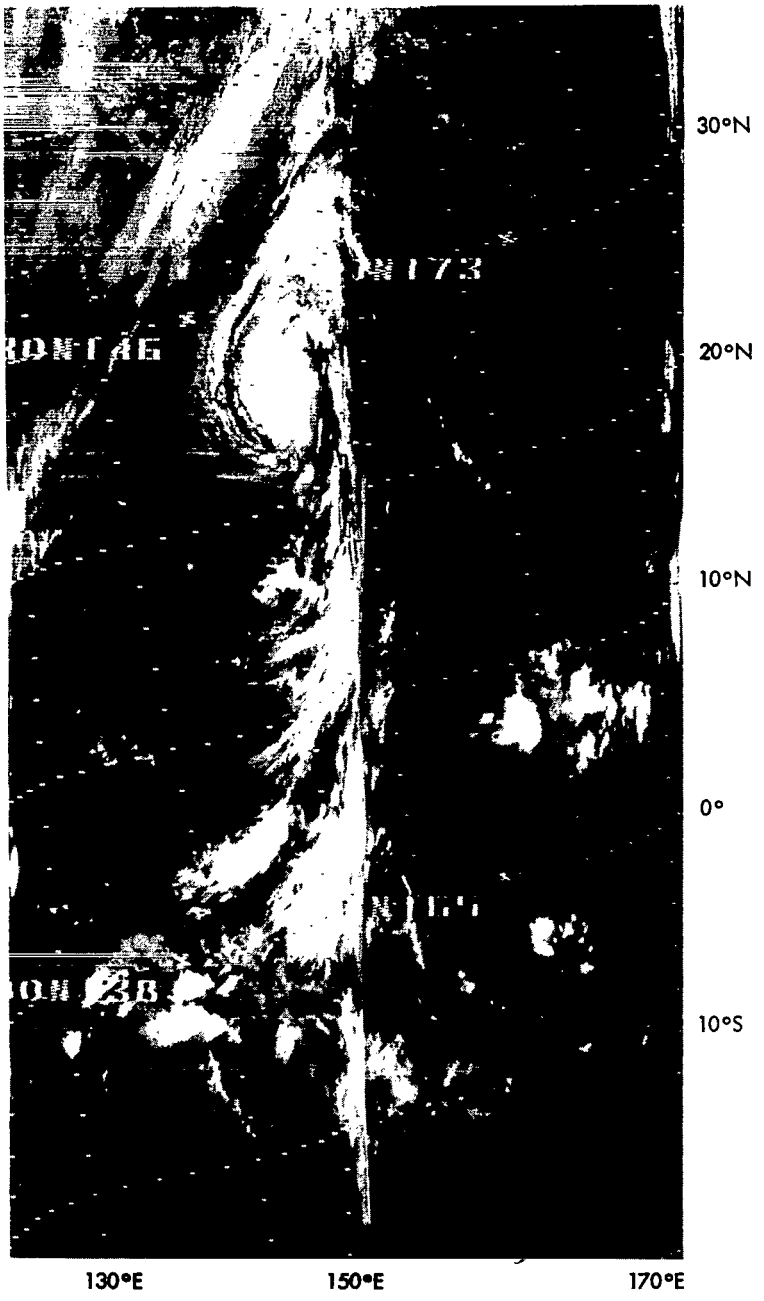


Figure J1—Montage of Nimbus II HRIR filmstrips (orbits 2279, and 2280) on November 2, 1966, near 1200 GMT (near local midnight).

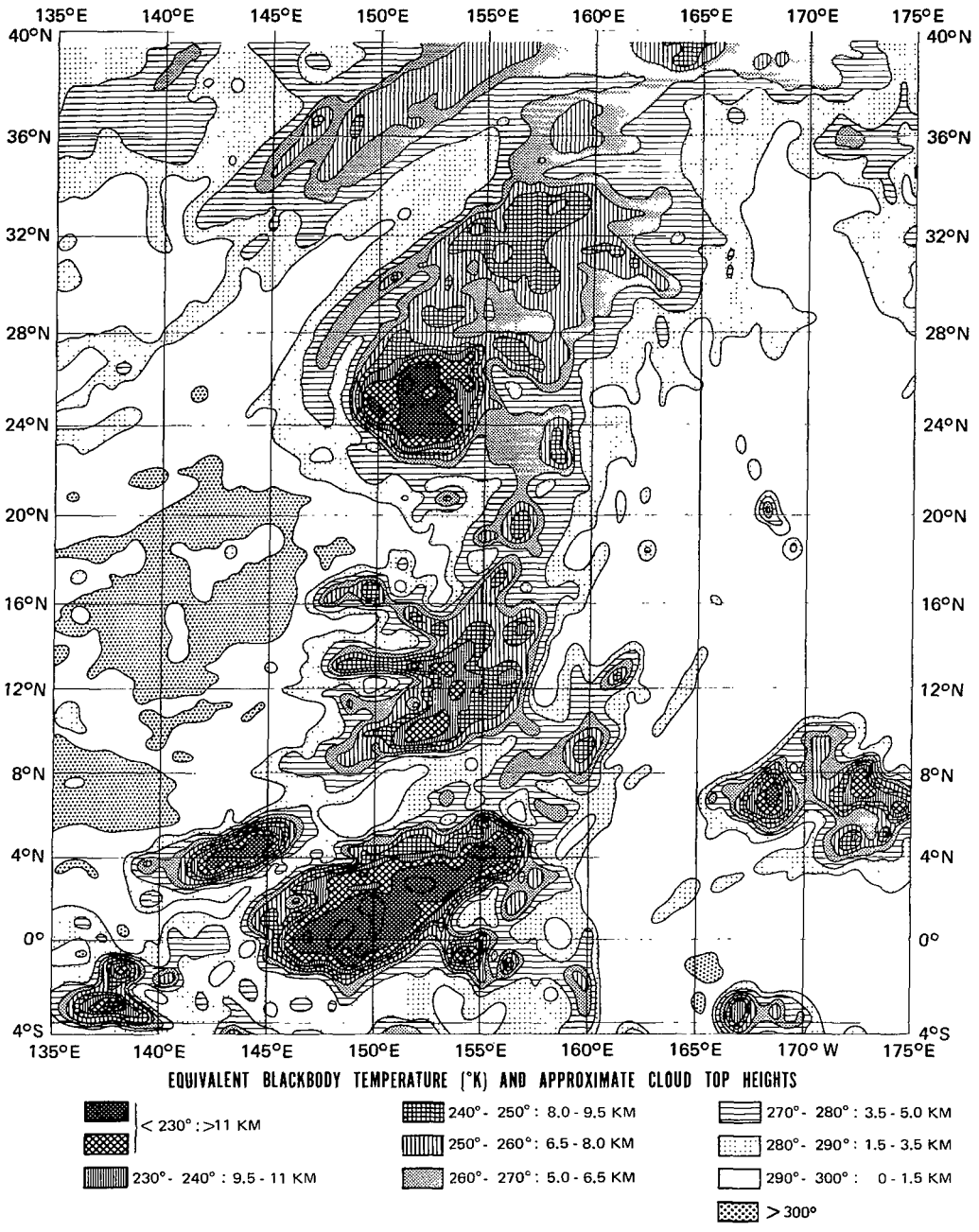


Figure J2—Analysis of Nimbus II HRIR measurements (orbits 2278, 2279, and 2280) on November 2, 1966, near 1200 GMT (near local midnight) based on a computer grid print map with 0.625 degree longitude per grid interval.

Appendix K

# November 3 through November 9, 1967

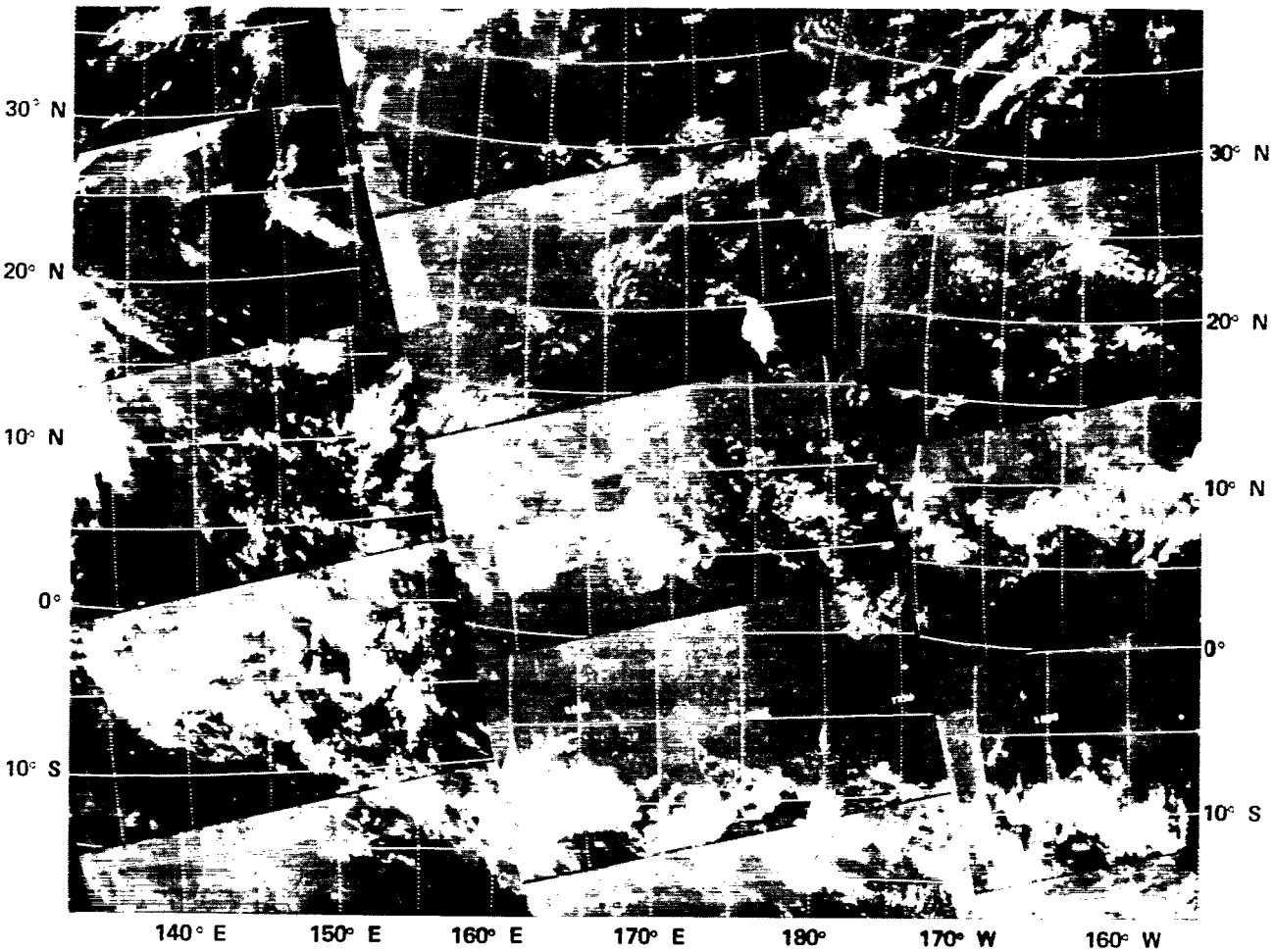


Figure K1. Montage of ESSA-3 Television Photographs (Orbits 4980, 4981, 4982) on 3 November 1967, near 0100 GMT (Local Early Afternoon)

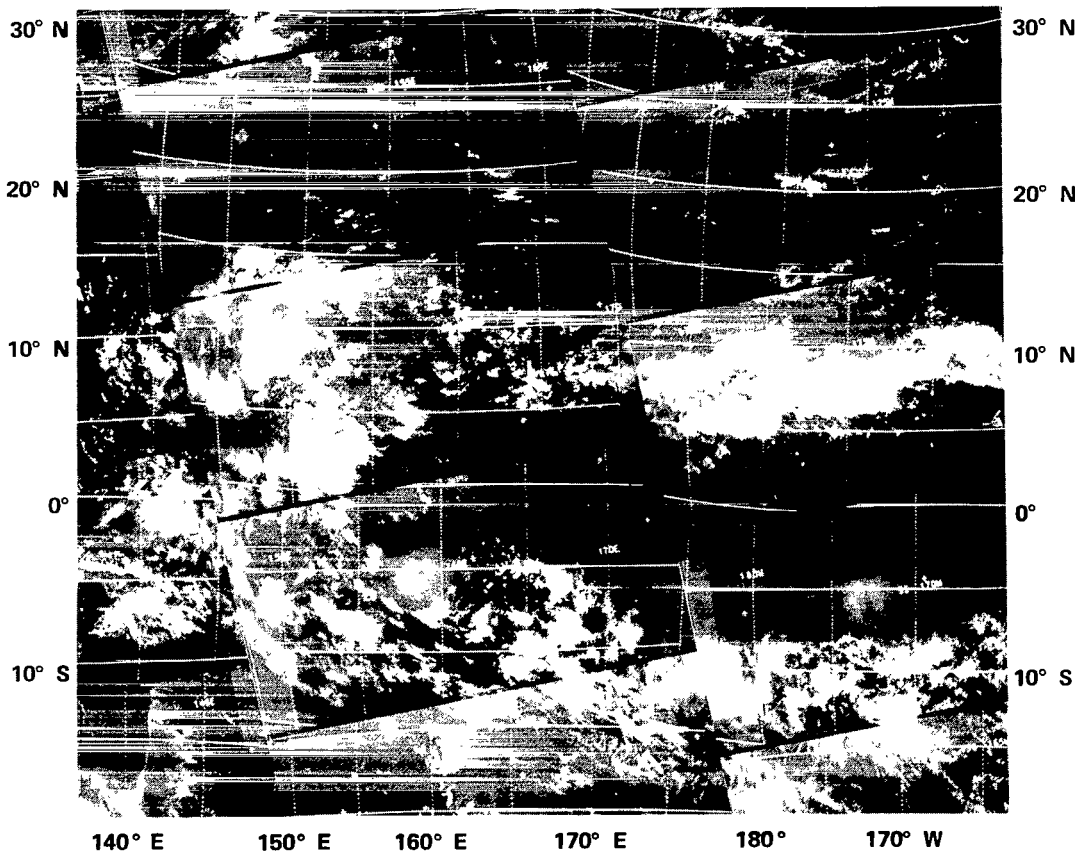


Figure K2. Montage of ESSA-3 Television Photographs (Orbits 4993, 4994, 4995) on 4 November 1967 near 0200 GMT (Local Early Afternoon)

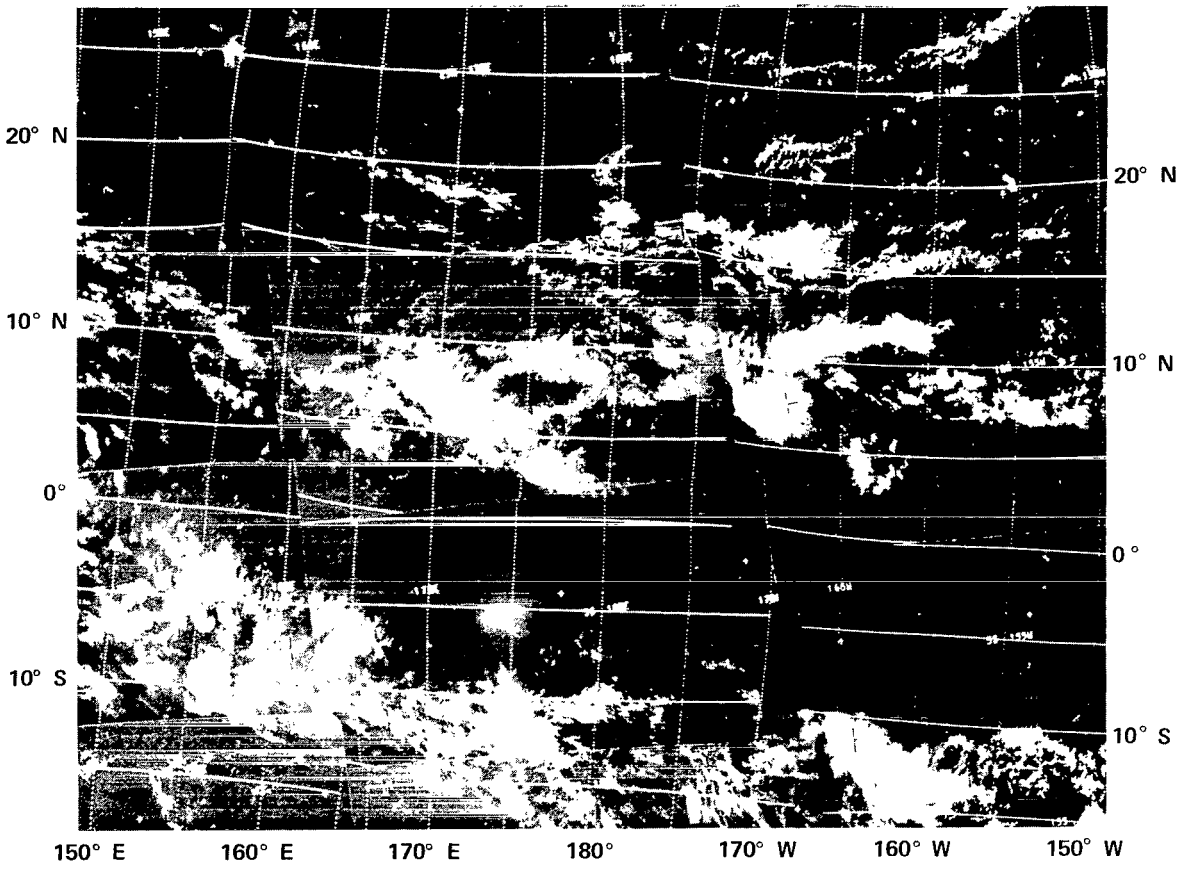


Figure K3. Montage of ESSA-3 Television Photographs (Orbits 5005, 5006, 5007) on 5 November 1967, near 0100 GMT (Local Early Afternoon)

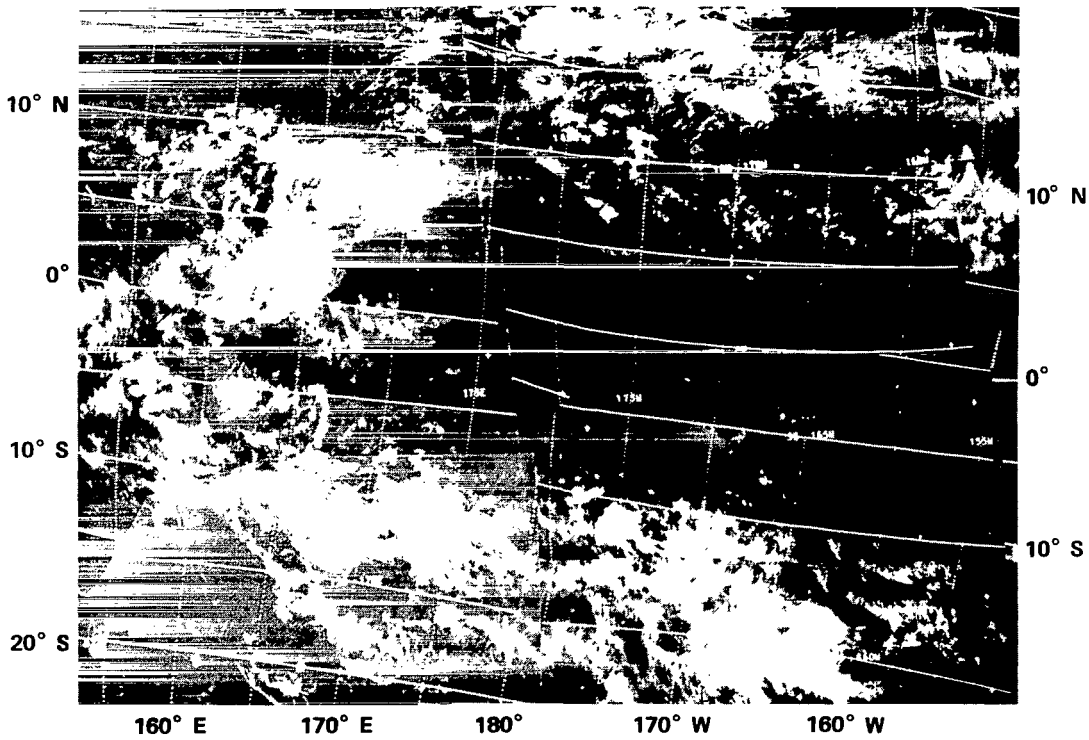


Figure K4. Montage of ESSA-3 Television Photographs (Orbits 5018, 5019) on 6 November 1967, near 0D00 GMT (Local Early Afternoon)

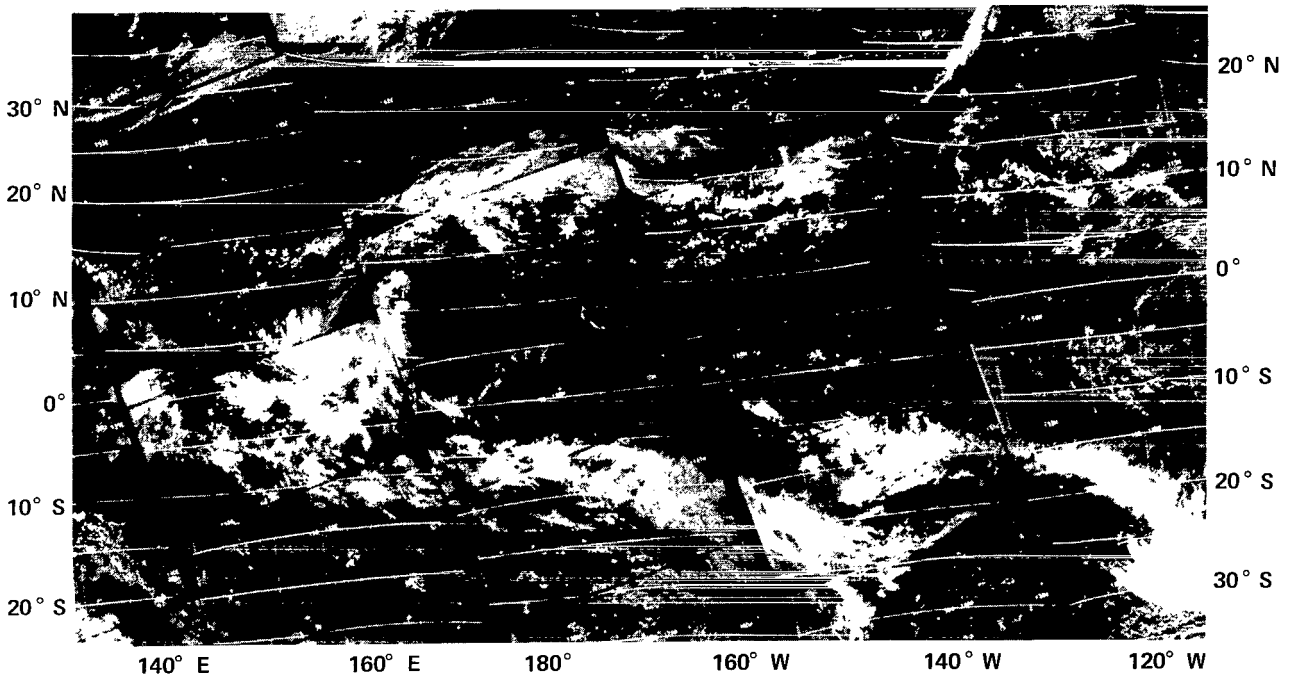


Figure K5. Montage of ESSA-3 Television Photographs (Orbits 5031, 5032, 5033) on 7 November 1967, near 0200 GMT (Local Early Afternoon)

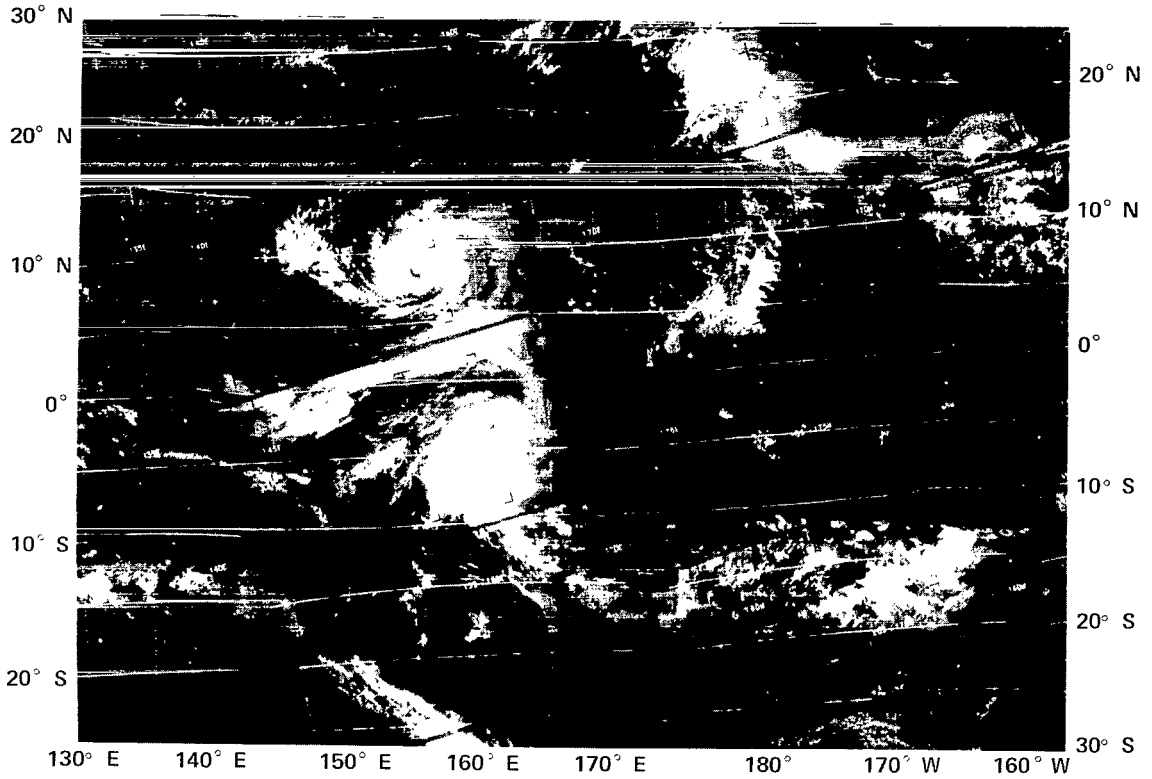


Figure K6. Montage of ESSA-3 Television Photographs (Orbits 5044, 5045, 5046) on 8 November 1967, near 0200 GMT (Local Early Afternoon)

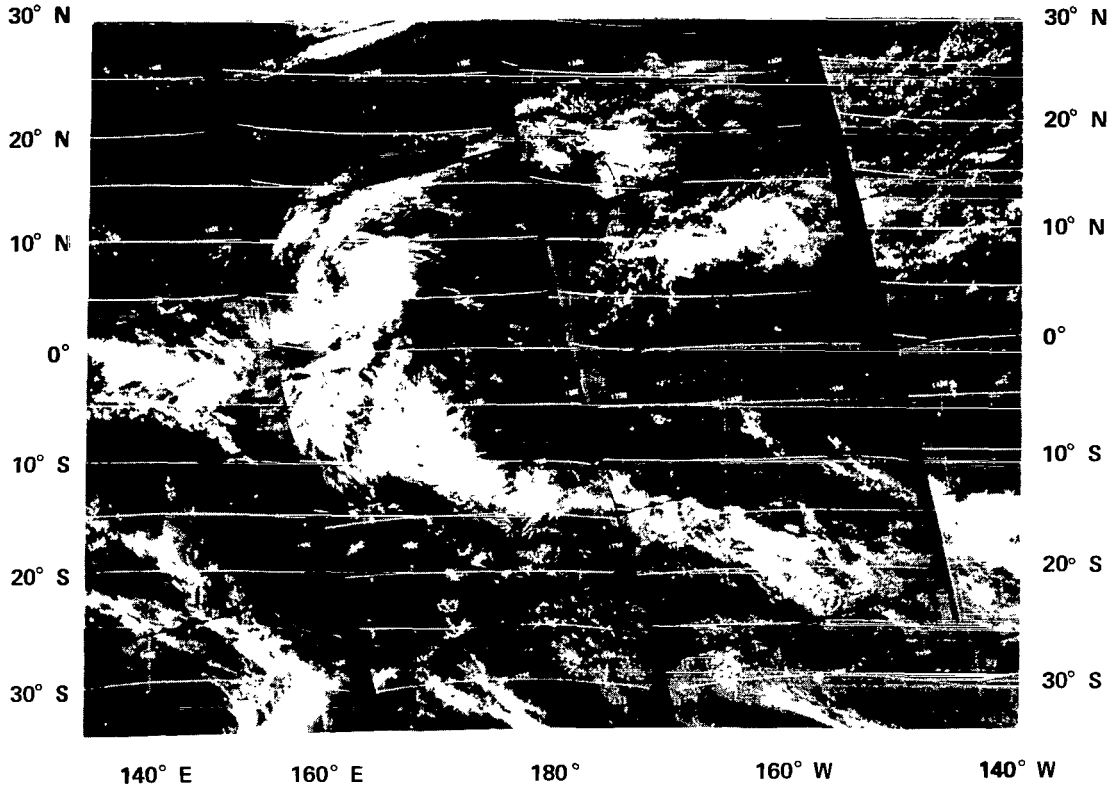


Figure K7. Montage of ESSA-3 Television Photographs (Orbits 5056, 5057, 5058) on 9 November 1967, near 0200 GMT (Local Early Afternoon)

*"The aeronautical and space activities of the United States shall be conducted so as to contribute . . . to the expansion of human knowledge of phenomena in the atmosphere and space. The Administration shall provide for the widest practicable and appropriate dissemination of information concerning its activities and the results thereof."*

—NATIONAL AERONAUTICS AND SPACE ACT OF 1958

# NASA SCIENTIFIC AND TECHNICAL PUBLICATIONS

TECHNICAL REPORTS: Scientific and technical information considered important, complete, and a lasting contribution to existing knowledge.

TECHNICAL NOTES: Information less broad in scope but nevertheless of importance as a contribution to existing knowledge.

TECHNICAL MEMORANDUMS: Information receiving limited distribution because of preliminary data, security classification, or other reasons.

CONTRACTOR REPORTS: Scientific and technical information generated under a NASA contract or grant and considered an important contribution to existing knowledge.

TECHNICAL TRANSLATIONS: Information published in a foreign language considered to merit NASA distribution in English.

SPECIAL PUBLICATIONS: Information derived from or of value to NASA activities. Publications include conference proceedings, monographs, data compilations, handbooks, sourcebooks, and special bibliographies.

TECHNOLOGY UTILIZATION PUBLICATIONS: Information on technology used by NASA that may be of particular interest in commercial and other non-aerospace applications. Publications include Tech Briefs, Technology Utilization Reports and Notes, and Technology Surveys.

*Details on the availability of these publications may be obtained from:*

**SCIENTIFIC AND TECHNICAL INFORMATION DIVISION**

**NATIONAL AERONAUTICS AND SPACE ADMINISTRATION**

**Washington, D.C. 20546**